Coordination Chemistry Reviews 253 (2009) 2980–2997

Contents lists available at ScienceDirect

Coordination Chemistry Reviews

journal homepage: www.elsevier.com/locate/ccr

Review

# Metal-organic coordination compounds for potential ferroelectrics

Wen Zhang, Heng-Yun Ye, Ren-Gen Xiong*

*Ordered Matter Science Research Center, Southeast University, Nanjing 211189, PR China*

**Contents**



ARTICLE INFO

*Article history:*
Received 9 January 2009
Accepted 25 February 2009
Available online 10 March 2009

ABSTRACT

A summary of recent work is presented describing the synthesis and characterization of noncentrosymmetric or homochiral metal-organic coordination compounds (MOCCs) or metal-organic coordination polymers (MOCPs) which belong to 10 polar point groups with potential ferroelectric properties. Under the guidance of structure–function relationship, by using homochiral organic ligands as building blocks

* Corresponding author. Tel.: +86 25 52090626; fax: +86 25 52090626.
*E-mail address:* xiongrg@seu.edu.cn (R.-G. Xiong).

0010-8545/$ – see front matter 
doi:10.1016/j.ccr.2009.02.028

*Keywords:*
Ferroelectricity
Polarization
Polar point groups
Metal-organic coordination compounds
Crystal structure
Homochirality
Hydrothermal reaction

or supramolecular crystal engineering strategies, a series of potential ferroelectric MOCCs (or MOCPs) has been assembled through coordinating bond formation. Their ferroelectric behavior is measured and evaluated. Also the future development of ferroelectrics based on MOCCs is outlined.



## 1. Introduction

Ferroelectrics are an interesting class of materials. It was discovered by Valasek in 1920 during the study of Rochelle salt ($NaKC_4H_4O_6{\cdot}4H_2O$, potassium sodium tartrate tetrahydrate) [1]. According to its crystal structure recently investigated by Solans et al. [2], the ferroelectric phase should be confined in the region between 255 and 297 K and its crystal system belongs to monoclinic $P2_1$ (polar point group $C_2$). Fifteen years later, Busch and Scherrer discovered $KH_2PO_4$ (KDP) and related materials which belong to H-bonded ferroelectrics, including Rochelle salt, as the first type of ferroelectrics [3]. In 1945, the first non-H-bonded ferroelectric $BaTiO_3$ was simultaneously discovered by Wul and Goldman in the Soviet Union [4] and von Hippel's group in the United States [5]. Until this discovery, it was assumed that hydrogen bonds were necessary for ferroelectricity to occur. Later, a significant progress in applications was made possible after the discovery of lead zirconate titanate – $Pb(Zr,Ti)O_3$ or PZT – with a large remanent ferroelectric polarization [6]. Since then, many pure inorganic compounds, liquid crystals and polymers have been explored and found a variety of technical applications in capacitors and in piezoelectric, pyroelectric, and optical devices, such as ferroelectric random access memories (FeRAM), ferroelectric field-effect transistors, infrared detectors, piezoelectric sensors, nonlinear optical devices and fast displays in electronic equipment [7].

Ferroelectrics may be defined as materials which show a spontaneous electric polarization and whose direction of the polarization can be reversed by an electric field. All ferroelectrics are piezoelectric and pyroelectric (see Fig. 1), but they additionally possess a reversible, non-volatile macroscopic spontaneous electric dipole moment in the absence of an external electric field. Experimentally, the reversal of the spontaneous polarization in ferroelectrics is observed as a single hysteresis loop, which may be measured through a Sawyer–Tower circuit [8a]. In order to understand the polarization–electric field ($P$–$E$) relationship (see Fig. 1), let us suppose that a ferroelectric crystal sample under test is initially composite of an equal number of positive and negative electric domains, which means that the net polarization of the crystal is equal to zero. When electric field is applied on the crystal, a curve composed of OA–AB–BC–CD–DF–FG–GH–HC is obtained. The portion OA of the curve shows a linear relationship between $P$ and $E$ when the electric field applied in the positive direction is not large enough, corresponding to the process that none of the domains is switched and the crystal behaves like a normal dielectric. With the increase of the electric field strength, a number of the negative domains switch over in the positive direction and the polarization increases rapidly (portion AB). The portion BC means a state of saturation reached where all the domains are aligned in the positive direction and the crystal consists of a single domain. When decreasing the field strength to zero, the polarization does not return to zero but rather follow the path CD to exhibit a remanent polarization $P_r$ (OD) because some of the domains remain aligned in the positive direction. The extrapolation of the linear portion BC of the curve back to the polarization axis offers the value of the spontaneous polarization $P_s$ (OE). An additional electric field in the opposite (negative) direction, called the coercive field $E_c$ (OF), is needed to annihilate the $P_r$ of the crystal to zero. Further increase of the field in the negative direction and reverse of the field direction once again complete the cycle. The resulting hysteresis loop (CDGHC) is the most important characteristic of the ferroelectric crystal. Obviously, ferroelectric materials are similar phenomenologically to ferromagnetic materials in that they exhibit hysteresis loops, spontaneous polarization, and coercive field.

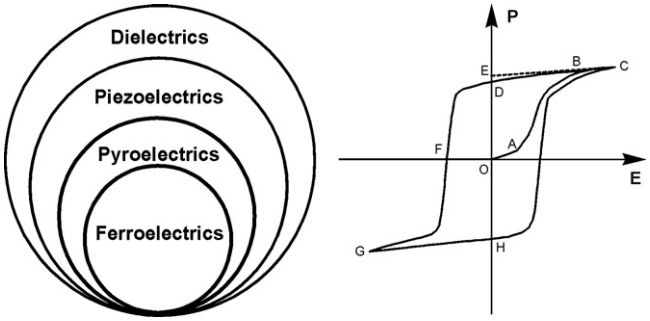


**Fig. 1.** Inter-relationships of ferroelectrics, pyroelectrics, piezoelectrics and dielectrics and ferroelectric hysteresis loop (polarization *vs.* applied electric field, i.e., $P$–$E$) [8a].

According to the definition, the ferroelectric material must possess a permanent dipole moment and this moment must be reversible in the presence of an applied voltage. The former requires the adoption of a space group that is associated with one of the ten polar point groups ($C_1$, $C_s$, $C_2$, $C_{2v}$, $C_3$, $C_{3v}$, $C_4$, $C_{4v}$, $C_6$, $C_{6v}$). The polar state is a consequence of the structural transition from a high-temperature, high-symmetry paraelectric phase to a low-temperature, low-symmetry ferroelectric phase. A dielectric anomaly at the Curie temperature where a maximum in the dielectric constant is often observed, indicating a phase transition between paraelectric and ferroelectric phases.

At present more than 300 ferroelectric substances are known. According to their chemical composition and their crystallographic structure, these substances can be classified into oxides, inorganic crystals other than oxides, organic crystals, liquid crystals, and polymers. Conventional materials achieving ferroelectricity can be roughly divided into three categories on a microscopic level: (I) order–disorder type, (II) displacive type, and (III) indirect type. The $KH_2PO_4$ (KDP) family is the typical example of type (I), in which the transfer of protons in the O–H···O bonds switches the spontaneous polarization. Another example is dipolar molecules such as $NaNO_2$, where the permanent dipoles generate spontaneous polarization and their reorientation generates the ferroelectricity. Many ferroelectric oxides such as $BaTiO_3$ belong to type (II), in which the relative displacement of ions creates spontaneous polarization.

Much of the attention in this field has been focused on developing ferroelectric and high-dielectric inorganic compounds such as KDP, $BaTiO_3$, $LiNbO_3$ and $CaCu_3Ti_4O_{12}$ [8b]. However, studies toward developing ferroelectric and dielectric materials based on metal-organic coordination compounds (MOCCs) have remained

**Table 1**
Ferroelectric properties of acentric or homochiral MOCCs or MOCPs.

| Compound code | Structure motif | Crystal system | Point group | Space group | $P_r$ ($\mu C\,cm^{-2}$) | $E_c$ ($kV\,cm^{-1}$) | Ref. |
|---|---|---|---|---|---|---|---|
| **1** | 0D | *2* | $C_2$ | $P2_1$ | 6.2 | 18 | [11] |
| **2** | 0D | *2* | $C_2$ | *I*2 | 0.6 | 20 | [12] |
| **3** | 0D | *2* | $C_2$ | $P2_1$ | 0.0021 | 0.8 | [13] |
| **4a** | 0D | *1* | $C_1$ | *P*1 | 0.25 | 12 | [16] |
| **4b** | 0D | *1* | $C_1$ | *P*1 | 0.46 | 14 | [16] |
| **5a** | 0D | *2* | $C_2$ | $P2_1$ | 0.0055 | 0.05 | [17] |
| **5b** | 0D | *2* | $C_2$ | $P2_1$ | 0.006 | 0.05 | [17] |
| **6** | 0D | *2* | $C_2$ | $P2_1$ | 0.11–0.32 | 8.5–20 | [18] |
| **7** | 1D | *mm2* | $C_{2v}$ | *Aba*2 | 0.28 | 10 | [19] |
| **8** | 3D | *m* | $C_s$ | *Cc* | 0.18–0.28 | 12 | [20] |
| **9** | 0D | *4* | $C_4$ | $P4_1$ | 0.2 | 0.8 | [21] |
| **10** | 3D | – | – | Acentric[a] | – | – | [22] |
| **11** | 3D | *222* | $D_2$ | *F*222 | 0.041 | 17.5 | [24] |
| **12** | 3D | – | $C_{\infty v}$ | – | 0.036 | 5.5 | [25] |
| **13** | 3D | – | – | Acentric[a] | – | – | [26] |
| **14** | 2D | *mmm* | $D_{2h}$[b] | *Pnma* | 0.001 | 1.5 | [27] |
| **15** | 3D | *mm2* | $C_{2v}$ | *Ima*2 | 0.027 | 1.88 | [28] |
| **16** | 3D | *mm2* | $C_{2v}$ | *Fdd*2 | 0.036 | 5.5 | [29] |
| **17** | 3D | *mm2* | $C_{2v}$ | *Fdd*2 | 0.004 | 2.5 | [30] |
| **18a** | 1D | *2* | $C_2$ | *C*2 | 0.28 | 16 | [31] |
| **18b** | 1D | *2* | $C_2$ | *C*2 | 0.14 | 12 | [31] |
| **18c** | 2D | *2* | $C_2$ | *C*2 | 0.12 | 5.0 | [32] |
| **18d** | 2D | *2* | $C_2$ | *C*2 | – | – | [32] |
| **18e** | 3D | *3* | $C_3$ | *P*3 | 1.4–2.5 | 0.65–1.0 | [33] |
| **19** | 1D | *1* | $C_1$ | *P*1 | 0.04 | 25 | [34] |
| **20a** | 1D | *2* | $C_2$ | $P2_1$ | 0.16 | 25 | [35] |
| **20b** | 1D | *2* | $C_2$ | $P2_1$ | 0.17 | 25 | [35] |
| **21** | 2D | *2* | $C_2$ | $P2_1$ | 0.12 | 5 | [36] |
| **22** | 2D | *2* | $C_2$ | $P2_1$ | 0.001 | 0.14 | [37] |
| **23** | 3D | *m* | $C_s$ | *Cc* | 0.38 | 2.10 | [38] |
| **24** | 3D | *mm2* | $C_{2v}$ | *Fdd*2 | 0.006 | 0.9–1.1 | [39] |
| **25a** | 2D | *2* | $C_2$ | *C*2 | 0.025 | 0.15 | [40] |
| **25b** | 2D | *2* | $C_2$ | *C*2 | 0.09 | 0.24 | [40] |
| **26a** | 2D | *2* | $C_2$ | *C*2 | 0.25 | 0.2 | [41] |
| **26b** | 2D | *2* | $C_2$ | *C*2 | 0.90 | 0.33 | [41] |

[a] The compound displays phase transfer, and there are no ferroelectric data in detail.
[b] Non-polar point group.

relatively sparse. It is strange because the first ferroelectrics Rochelle salt is actually *a real MOCC*.

The synthesis (or self-assembly) and design of novel materials based upon MOCCs have achieved much success recently due to the development of supramolecular crystal engineering. It prompted us to synthesize MOCCs falling in one of the ten polar point groups by exploiting the strong and highly directional metal–ligand coordination bonds. MOCCs or metal-organic hybrid materials bear the advantages of the organic ligands and inorganic ions. The organic component possesses the tailorability, π-conjugation and chirality while the inorganic metal ion possesses the hybrid orbital diversity (d and f orbits combined into coordination bonds) and electronic, magnetic and optical properties [9]. Noncentrosymmetric (acentric) or homochiral MOCCs with desired configuration or topologies can be rationally designed by taking advantage of well-defined metal coordination geometries in combination with carefully chosen bend (or kink) or homochiral ligands. We here wish to describe our successful development of several crystal engineering strategies toward the synthesis of acentric or homochiral MOCCs that can crystallize in one of the ten polar point groups. These compounds are attractive targets as they can potentially display ferroelectric properties with high-dielectric constants and ferroelectric properties.

We will describe three sections in detail on the basis of the chirality or acentric origins of MOCCs (see Scheme 1 and Table 1): (I) homochiral discrete or zero-dimensional (0D) MOCCs; (II) acentric metal-organic coordination polymers (MOCPs) produced through supramolecular crystal engineering strategy; (III) homochiral MOCPs constructed by homochiral organic ligand as building blocks.

## 2. Homochiral discrete or zero-dimensional MOCCs

To describe a discrete MOCC, it is necessary to give a brief introduction of three typical ferroelectrics: Rochelle salt, KDP and triglycine sulfate (TGS).

The well-known oldest ferroelectric crystal is Rochelle salt [2] (see Fig. 2). The most outstanding property of Rochelle salt is that it exhibits two Curie points. The space group below 255 K and above 297 K is orthorhombic $P2_12_12$, corresponding to the paraelectric phase while between the temperature range the space group is monoclinic $P2_1$, corresponding to the ferroelectric phase. The paraelectric–ferroelectric transition is of the order–disorder type.

In the crystal structure, there are rows of tartrate ions parallel to the *a* axis, linked along the *b* axis by rows of alternating K and Na ions. Every tartrate ion is surrounded by six tartrate ions. K and Na ions act as a bridge among tartrate ions. The K ions adopt a bicapped trigonal prism geometry and the Na ions display a distorted octahedral geometry via the coordination with the O atoms from acetate, OH and water. The crystal structure of Rochelle salt is a combination of two kinds of different chains along the *a* axis. The main difference among the ferroelectric structure and the two paraelectric structures is in the orientation of each tartrate ion with respect to the crystallographic axes. It is assumed that the ferroelectricity is produced by two nonequivalent chains along the *a* axis, each with a different polarization vector parallel to the *a* axis.

As well-known hydrogen-bonded ferroelectrics, the pure inorganic compound KDP has been the most intensively studied over the second half of the last century [3]. There are extensive hydrogen bonds in its structure that gives rise to a diamondoid network (see Fig. 2).

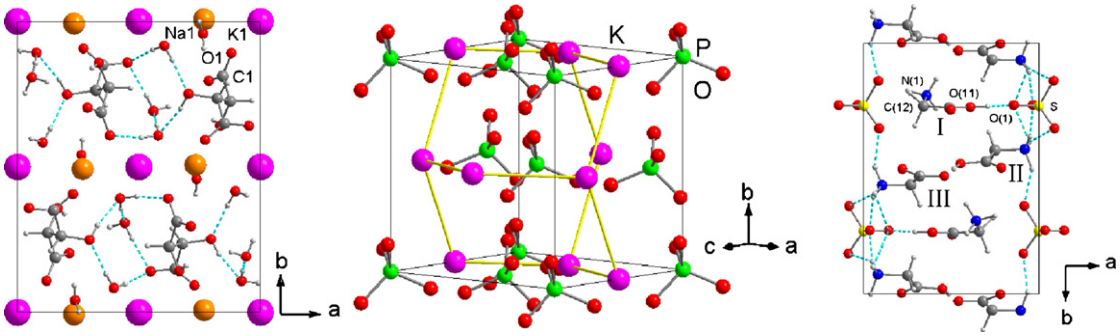


**Fig. 2.** Views of the unit cell content of Rochelle salt (paraelectric phase) (left) [2], KDP (paraelectric phase) (middle) [3] and TGS (ferroelectric phase) (right) [10a].

**(I) homochiral discrete or zero-dimension (0D) MOCCs**

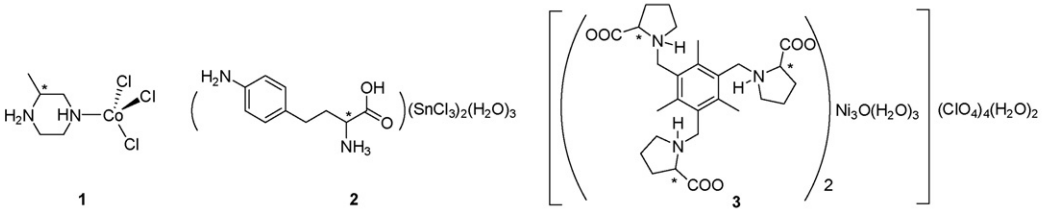


**(II) acentric MOCPs produced through supramolecular crystal engineering strategy**

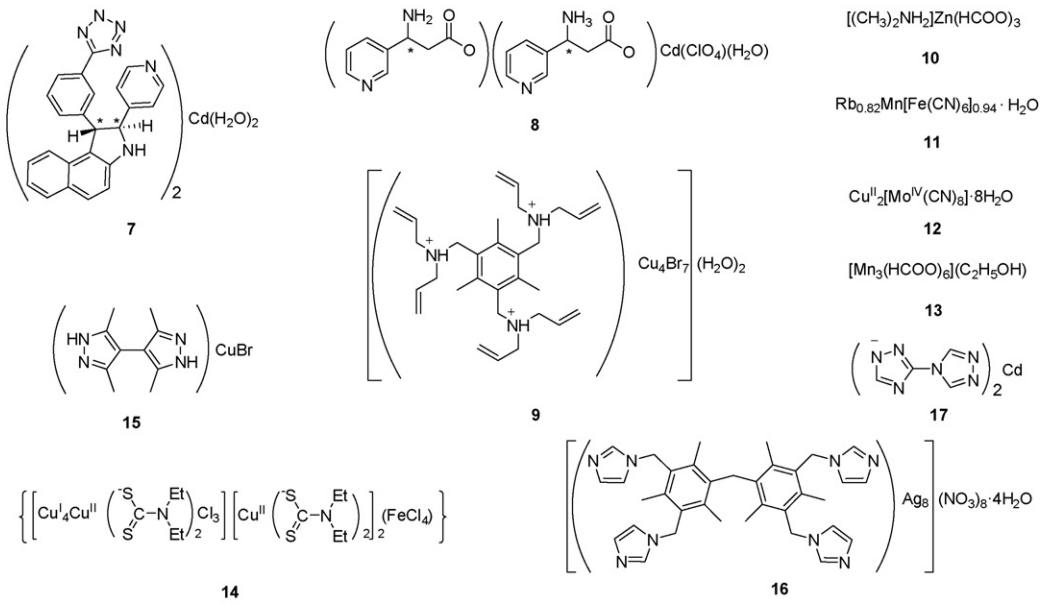


**Scheme 1.** (I) Homochiral discrete or zero-dimension (0D) MOCCs. (II) Acentric MOCPs produced through supramolecular crystal engineering strategy. (III) Homochiral MOCPs constructed by homochiral organic liagnds.

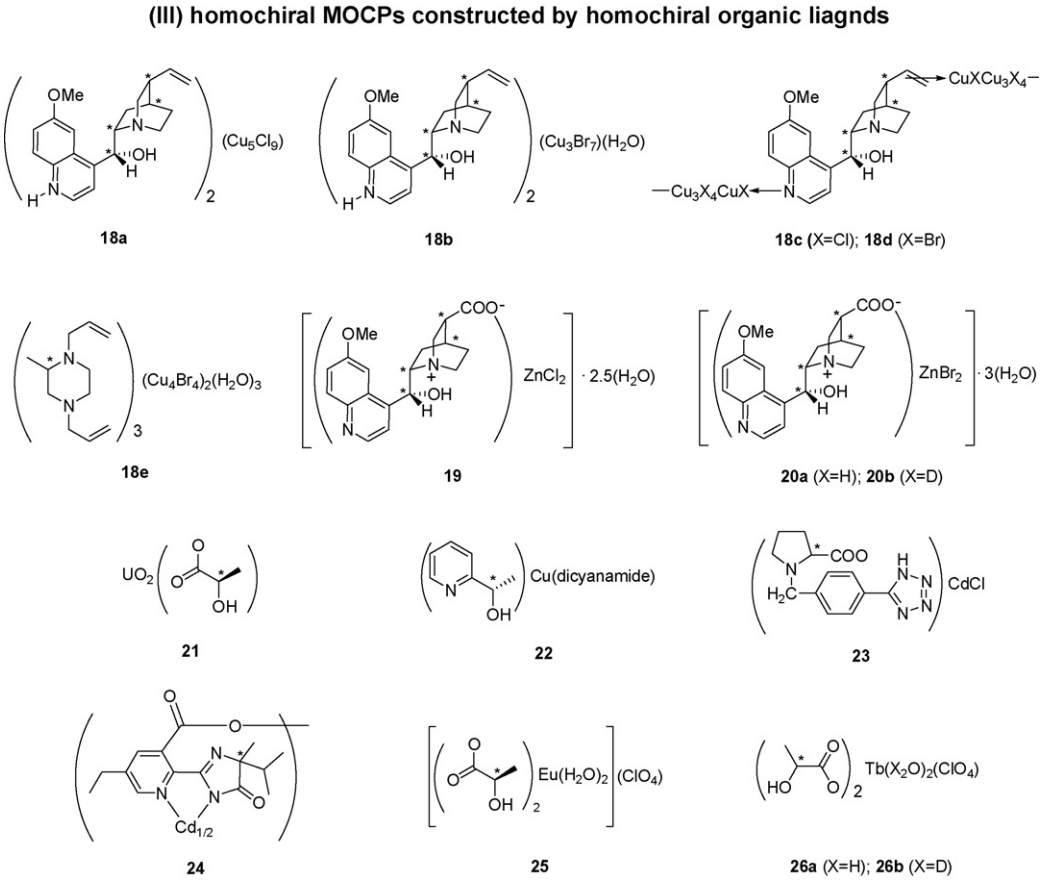


**Scheme 1.** (*Continued*).

KDP undergoes the paraelectric–ferroelectric phase transition at 123 K. The paraelectric phase adopts the tetragonal space group $I^{-}42d$ (point group $D_{2d}$) where the ferroelectric phase adopts the orthorhombic space group *Fdd*2 (polar point group $C_{2v}$). The spontaneous polarization of KDP arises from the collective site-to-site transfer of protons in the O–H···O bonds, along with the displacive deformation of $PO_4^{3-}$ ions. Upon deuteration, KDP shows a huge isotopic effect of *Curie temperature* with an increase of about 90 K.

TGS is another typical ferroelectric discovered by Matthias et al. in 1956 [10a]. It is synthesized from amino acid glycine and sulfuric acid. In the crystal structure, there are three types of glycine molecules, i.e., I, II and III (see Fig. 2). The structural formula of TGS can be best written as $[(H_3N^+CH_2COOH)_2(H_3N^+CH_2COO^-)\cdot SO_4^{2-}]$, among which the glycinium ion $H_3N^+CH_2COOH$ corresponds to glycines I and II while the zwitterion $H_3N^+CH_2COO^-$ to glycine III. The C, N and O atoms in glycine II and III locate almost in plane while the N atom in glycine I deviates of *ca.* 0.27 Å from the OCO plane. The sulfate exhibits a distorted tetrahedral geometry. The glycines and sulfate ions are connected through hydrogen bonds. The direction of spontaneous polarization $P_s$ is due to the orientation of the polar group $NH_3^+$ of glycine I molecule along the *b* axis.

TGS displays a perfect hysteresis loop along the *b* axis and its $P_s$ reaches 3.5 μC cm$^{-2}$ at room temperature. It shows a typical second order ferroelectric phase transition at Curie temperature of 322 K. The paraelectric phase is monoclinic $P2_1/m$ belonging to the centrosymmetrical class 2/m while the ferroelectric phase below the transition temperature is monoclinic $P2_1$ belonging to the polar point group 2. TGS crystal is one of the best materials for use as a sensitive element in room temperature infrared detectors and imaging systems due to its excellent ferroelectric and pyroelectric properties [10b].

### 2.1. *[Co(II)Cl$_3$(H-MPPA)] (**1**)*

[Co(II)Cl$_3$(H-MPPA)] (**1**) is one of the successful ferroelectric examples where its electric hysteresis loop reaches perfect spontaneous polarization status since the exploration of potential ferroelectrics based on MOCCs [11]. Compound **1** was prepared through the reaction of dichloride (*R*)-2-methylpiperazine (MPPA) bi-cation with $CoCl_2$.

X-ray crystal structural determination clearly shows that the local coordination environment around Co center is a distorted tetrahedron composed of three terminal Cl atoms and one N atom from unprotonated N atom of MPPA (see Fig. 3). One of the N atoms from MPPA ligand is protonated and loses its coordination ability. Thus, three H atoms (H1, H2A and H2B) form hydrogen bonds between three Cl atoms (Cl1, Cl2 and Cl3) to lead to the formation of 3D framework created through hydrogen bonds (as shown in Fig. 3). A careful investigation shows that three bond distances

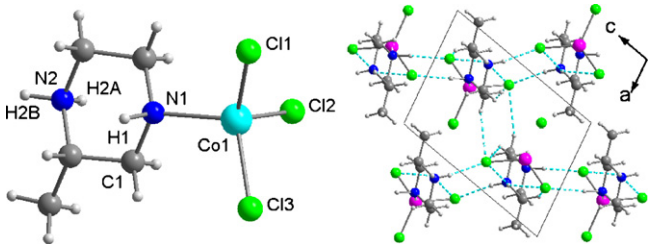


**Fig. 3.** Molecular structure of crystal state of [CoCl$_3$(H-MPPA)] (**1**) and its 3D packing view along the *b* axis [11].

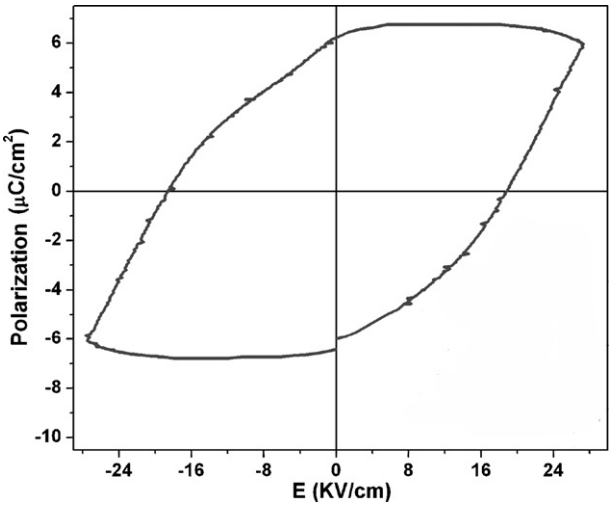


**Fig. 4.** Electric hysteresis loop of [Co(II)$Cl_3$(H-MPPA)] (**1**) recorded at room temperature [11].

of Co–Cl are not equal to each other and display some differences (Co–Cl1 = 2.225 Å; Co–Cl1 = 2.283 Å; Co–Cl1 = 2.260 Å). As expected, the bond distance of $Co_1$–$N_1$ is in the normal range of Co–N bond lengths. The piperazine ring adopts a stable chair-type conformation.

As **1** crystallizes in a chiral space group $P2_1$ which belongs to one of the ten polar point groups ($C_2$), its ferroelectric property would occur in principle. The single crystal with an approximate dimension of 0.40 mm × 0.35 mm × 0.26 mm was carefully selected with electrodes on approximate crystallographic faces (0 1 0). Fig. 4 clearly shows that an electric hysteresis loop was observed when the applied electric field was set at about 28 kV $cm^{-1}$. A spontaneous polarization ($P_s \approx 6.8\ \mu C\ cm^{-2}$) occurred in the measuring conditions and remanent polarization ($P_r \approx 6.2\ \mu C\ cm^{-2}$) was almost equal to that of $P_s$. $P_s$ of **1** was high as almost twice as that of TGS ($P_s = 3.5\ \mu C\ cm^{-2}$) and significantly larger than that of KDP. As we know, compound **1** is the first example of ferroelectric MOCC that can really reaches the spontaneous polarization status. The direction of the spontaneous polarization in the ferroelectric phase of **1** may be perpendicular to the chains and to the Cl···HN hydrogen bonds, analogically as in KDP and other KDP-type ferroelectrics. Compound **1** is a good ferroelectric candidate and opens up a new avenue to explore novel MOCCs-based ferroelectrics containing hydrogen bonds.

### 2.2. $[NH_3C_6H_4(CH_2)_2CHNH_3COOH](SnCl_3)_2{\cdot}(H_2O)_3$ (**2**)

The H-bonded MOCC $[NH_3C_6H_4(CH_2)_2CHNH_3COOH](SnCl_3)_2{\cdot}(H_2O)_3$ (**2**) was obtained during the preparation of (*S*)-4-(4′-aminophenyl)-2-aminobutanoic acid by the reduction of (*S*)-2-amino-4-(4′-nitrophenyl)butyric acid (NOHPA) in the presence of $SnCl_2$ and HCl (see Fig. 5) [12].

Compound **2** crystallizes in a space group *I*2 (polar point group $C_2$), a prerequisite for a ferroelectric. Its crystal structure was

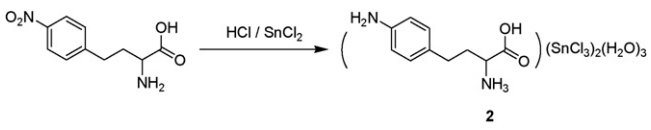


**Fig. 5.** Synthesis of **2** showing the reduction of (*S*)-2-amino-4-(4′-nitrophenyl)butyric acid in the presence of $SnCl_2$ and HCl [12].

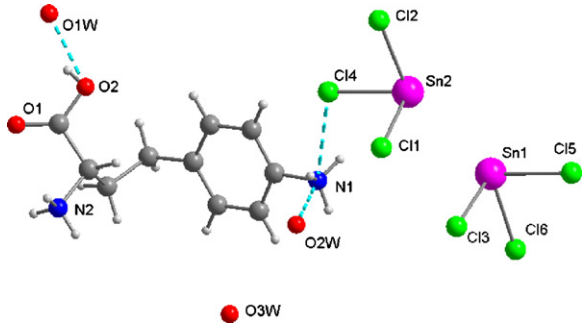


**Fig. 6.** Asymmetric unit representation of **2** [12].

disclosed by an X-ray single crystal diffraction investigation. The asymmetric unit contains two crystallographically unique $SnCl_3^-$ anions sharing a similar pseudo-trigonal pyramidal coordination environment (see Fig. 6). Interestingly, the reduction product of NOHPA is a cation, with both amino groups existing as ammonium groups and the carboxylate group protonated. The cation with the $NH_3^+$ group on the aliphatic chain and the free carboxylic acid in **2** resembles the two nonzwitterionic amino acids in TGS, which plays an important role in spontaneous polarization. In **2**, both ammonium groups participate in a number NH···Cl hydrogen bonds with $SnCl_3^-$ anions. The N···Cl separations are in the range 3.297(2)–3.330(2) Å. These H-bonding interactions result in the formation of a 3D pillar-layered network. Water molecules participate in two additional, strong hydrogen bonds that extend to the carboxylic acid and the aromatic amino group. The O···O and N···O separations are 2.561(2) and 2.694(2) Å, respectively. There is also direct hydrogen bonding between neighboring amino acids (2.894 Å), resulting in the formation of chains involving only amino acids that extend in the *b* direction.

Preliminary study of powdered pellet sample indicates that **2** displays an electric hysteresis loop which can be considered as a typical ferroelectric feature with a $P_r$ of *ca.* 0.60 μC $cm^{-2}$ and an $E_c$ of 20 kV $cm^{-1}$.

### 2.3. $[Ni_3(TBPLA)_2(\mu_3\text{-}O)](ClO_4)_4(H_2O)_5$ (**3**)

Another H-bonded discrete homochiral ferroelectric MOCC is $Ni_3(TBPLA)_2(\mu_3\text{-}O)(ClO_4)_4(H_2O)_5$ (**3**) (TBPLA = (*S*)-1,1′,1″-2,4,6-trimethylbenzene-1,3,5-triyl-tris(methylene)-tris-pyrrolidine-2-carboxylic acid), which was obtained by the hydrothermal reaction of $Ni(ClO_4)_2{\cdot}6H_2O$ with TBPLA (see Scheme 1) [13]. **3** crystallizes in a chiral space group $P2_1$ belonging to one of the ten polar point groups ($C_2$). The TBPLA ligand is a zwitterionic neutral molecule similar to the amino acid in TGS, and acts as a hexadentate chelator with each of the ligand's bidentate carboxylate moieties coordinated to the Ni atoms (see Fig. 7). The molecular charge of **3** is balanced by four free $ClO_4^-$ anions and one $\mu_3$-O atom. The TBPLA ligand takes an all-*cis* coordination mode resembling the shape of a parachute. Each Ni center displays a slightly distorted octahedron geometry which is composed of six O atoms, i.e., four of the O atoms from four different carboxylate groups and two from the oxo group and $H_2O$. Similarly, 3D framework occurs in **3** through strong H-bond (see Fig. 7).

Ferroelectric measurements of the powdered pellet sample show that the $P_r$ value is *ca.* $2.1 \times 10^{-3}$ μC $cm^{-2}$ and $E_c$ *ca.* 0.8 kV $cm^{-1}$. A leakage current occurred in high electric field during the measurement. One significant characteristic of **3** is the large permittivity anisotropy along three crystallographic axes. The dielectric anisotropy ratios of $\varepsilon_{r//c}/\varepsilon_{r//b}$ and $\varepsilon_{r//c}/\varepsilon_{r//a}$ are *ca.* 3.47 and 2.22, respectively, showing temperature-independence.

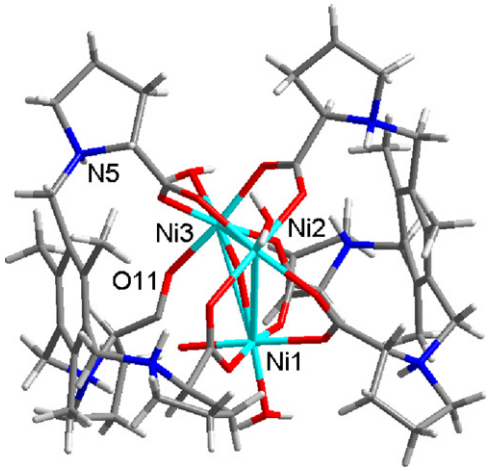


**Fig. 7.** Molecular structure of **3** where water and $ClO_4^-$ are omitted for clarity [13].

### 2.4. $[(CBCN_4)_2Zn_2Br_2(N_3)_2](X_2O)$ (**4a**, X = H; **4b**, X = D)

Taking into account of the above-mentioned samples, it can be seen that H-bond is responsible for ferroelectric behavior. It means that strengthening of H-bond is a prerequisite to enhancement of ferroelectric properties. It is worth noting that the deuterium effect (DEF) by exchanging hydrogen with deuterium on the hydrogen bonds plays a very important role not only in the enhancement of many physical properties such as nonlinear optical (especially second harmonic generation response), ferroelectricity and permittivity, but also in the basic theoretical point of view. Some of typical examples are found in pure organic and inorganic compounds. For example, Phz–$H_2$ca/Phz–$D_2$ca (Phz = phenazine, $H_2$ca = bromanilic acid) shows huge dielectric response with an increase of 50 K in the dielectric constant at 1 MHz as a function of temperature. A significant increase of dielectric DEF in phenylsquaric acid occurs from 8 to 18 [14]. KDP/DKDP ($KD_2PO_4$) exhibits dielectric DEF increase by 80% and ferroelectric $P_s$ increase by 24% [15].

The following one example of homochiral MOCC clearly shows a good deuterium effect on ferroelectricity. The novel Zn-dimer $[(CBCN_4)_2Zn_2Br_2(N_3)_2](X_2O)$ (**4a**, X = H; **4b**, X = D) was obtained by the reaction of *N*-4′-caynobenzylcinchonidine bromide (CBCBr) with $NaN_3$ in the presence of $ZnBr_2$ ($CBCN_4$ = *N*-4′-tetrazoylbenzylcinchonidine) (see Fig. 8) [16]. X-ray crystal structural determinations of **4a** and **4b** reveal that the local coordination geometry around each Zn center can be best described as a slightly distorted tetrahedron which is composed of three N atoms (two from tetrazoyl group and one from terminal azide) and one terminal Br atom (see Fig. 9). Two tetrazoyl groups link two Zn centers to form a dimer. In both **4a** and **4b**, the pyridyl group of quinoline ring fails to bind to Zn atoms. Thus, each $CBCN_4$ ligand acts as bidentate chelator by using 1,2-$\mu_2$-tetrazoyl groups. Both of **4a** and **4b** are isostructural and crystallize in chiral space group *P*1 belonging to polar point group $C_1$. Due to many H-bonds between O atom of 9-hydroxy group of $CBCN_4$ and N atom of azide or Br, and O atom of water or deuterated water and N atom of azide or tetrazoyl group, a 3D framework is formed. Interestingly, $CBCN_4$ in **4a** and **4b** is a zwitterion-like ion with long charge separation, which is essentially helpful for the formation of large $P_r$ or $P_s$ possibly.

Samples **4a** and **4b** display ferroelectric behaviors. Measurements clearly show there is an electric hysteresis loop in **4a** with a $P_r$ of *ca.* 0.25 μC cm$^{-2}$ and an $E_c$ of *ca.* 12 kV cm$^{-1}$. Similarly, the $P_r$ and $E_c$ of **4b** can be estimated to be 0.46 μC cm$^{-2}$ and 14 kV cm$^{-1}$, respectively. Thus, larger ferroelectric DEF (with an increase of $P_s$ of 40%) on ferroelectric behavior was detected between MOCCs **4a** and **4b**. Similarly, the large ferroelectric behavior was further con-

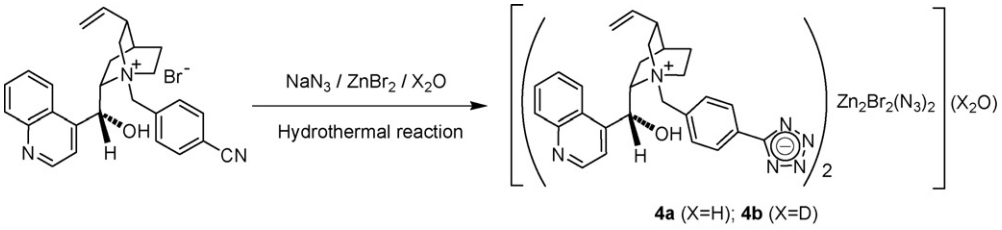


**Fig. 8.** Synthesis of **4a** (X = H) or **4b** (X = D) [16].

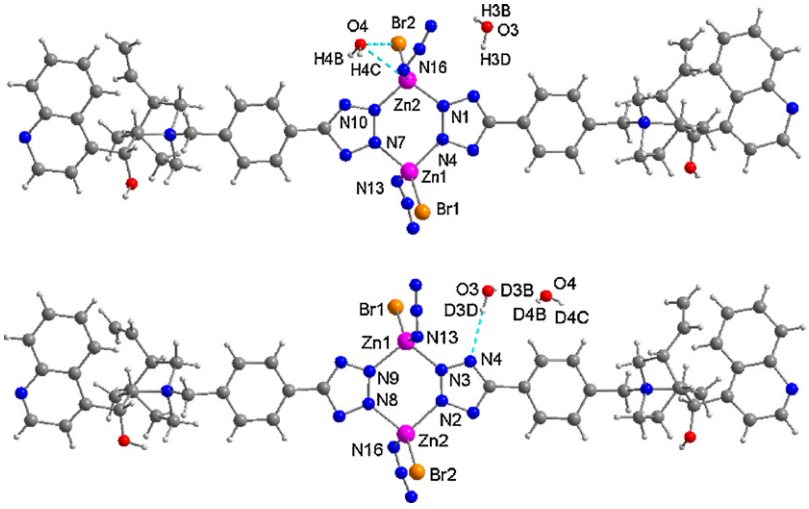


**Fig. 9.** Dimer representations of **4a** and **4b** [16].

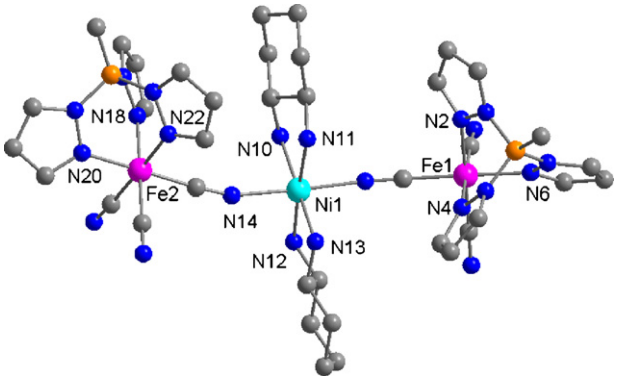


**Fig. 10.** Structure of **6a** [18].

firmed by their large dielectric constant (25.1 for **4a** and 69.1 for **4b** at low frequency).

### 2.5. *[(tta)$_3$(pbpy)Eu] ((R,R)-**5a**; (S,S)-**5b**)*

Strong geometry distortion around central metal ion will result in large charge separation to induce ferroelectric behavior like non-H-bonded ferroelectrics $TiBaO_3$. Two rare earth coordination compounds, [(tta)$_3$(pbpy)Eu] ((*R*,*R*)-**5a**; (*S*,*S*)-**5b**), were obtained by the reaction of [Eu(tta)$_3$]·2H$_2$O (tta = 2-thenoyltrifluoroacetonato) with chiral 4,5-pinene-bipyridine (pbpy). Both complexes may be non-H-bonded ferroelectrics (see Scheme 1) [17].

X-ray crystal structure determination reveals that both **5a** and **5b** crystallize in a chiral space group $P2_1$ belonging to the polar point group $C_2$. The central Eu atom is eight-coordinated with a strongly distorted square-antiprism geometry. A dominant feature is that the ferroelectric value measured on thin film ($P_r \approx 0.022\ \mu C\ cm^{-2}$) is significantly larger than that in powdered pellet sample ($P_r \approx 0.006\ \mu C\ cm^{-2}$) with an increase of *ca.* 270%. As expected, the ferroelectric behaviors of both **5a** and **5b** are basically identical because they are enantiomers. Their ferroelectric feature is also confirmed by the dielectric behavior.

### 2.6. *[(MeTp)$_2$Fe$_2$(CN)$_6$Ni(chxn)$_2$] ((R,R)-**6a**; (S,S)-**6b**)*

Two homochiral trinuclear clusters, [(MeTp)$_2$Fe$_2$(CN)$_6$Ni(chxn)$_2$] ((*R*,*R*)-**6a**; (*S*,*S*)-**6b**) (MeTp = methyltris(pyrazolyl)borate; chxn = (1*R*,2*R*)- or (1*S*,2*S*)-1,2-diaminocyclohexane), were prepared through the reaction of (1*R*,2*R*)-chxn or (1*S*,2*S*)-chxn with Ni(ClO$_4$)$_2$·6H$_2$O and (Bu$_4$N)[(MeTp)Fe(CN)$_3$] in a mixture of acetonitrile, methanol, and water [18].

The X-ray crystallography reveals that **6a** and **6b** are enantiomers with a space group $P2_1$ (polar point group $C_2$). Complex **6a** is a neutral trinuclear Fe$_2$Ni cluster and a central [Ni((1*R*,2*R*)-chxn)$_2$]$^{2+}$ core is linked to two [MeTpFe(CN)$_3$]$^-$ ions at *trans* positions via bridging cyanides with the Fe–Ni–Fe angle of 162.09(2)° (see Fig. 10). The nickel atom is six-coordinated in a distorted octahedral geometry constructed by four nitrogen atoms from two chair (1*R*,2*R*)-chxn ligands and two nitrogen atoms from two cyanide groups. Three cyanide ligands in a *fac* arrangement and a tridentate nitrogen-donor MeTp ligand form a distorted octahedral environment around the $Fe^{III}$ ion.

The ferroelectric property of **6a** was investigated, displaying a ferroelectric hysteresis loop with a $P_r$ of *ca.* 0.11–0.32 $\mu C\ cm^{-2}$ and an $E_c$ of *ca.* 8.5–20 $kV\ cm^{-1}$. The $\chi_M T$ data confirms a ferromagnetic coupling within the Fe$_2$Ni cluster, revealing that they are examples of metal-organic compounds bearing ferroelectricity and intramolecular ferromagnetic interactions.

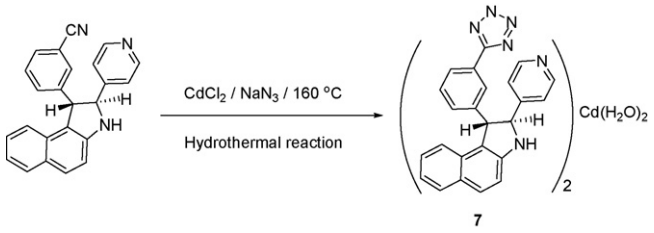


**Fig. 11.** Synthesis of **7** [19].

Compounds **1**–**5b** all contain zwiterion-like ligands resulting in the formation of intramolecular dipolar moments like in TGS. This gives us a hint that for the design of ferroelectric MOCCs, maybe amino-acid-like ligand is the best choice. For non-H-bonded MOCCs like **5a** and **5b**, they should contain central ions with high-coordination numbers who are labile to develop strong distortions.

## 3. Acentric MOCPs produced by supramolecular crystal engineering

### 3.1. *[Cd(L)$_2$(H$_2$O)$_2$] (**7**)*

In this section, we mainly focus on the discussion about potential ferroelectric MOCP constructed from non-homochiral organic ligands by crystal packing. One infinite acentric [Cd(L)$_2$(H$_2$O)$_2$] (**7**) probably represents the crystal engineering strategy to self-assemble ferroelectric MOCP. Compound **7** was obtained by the hydrothermal reaction of $CdCl_2$ with L (L = *trans*-2,3-dihydro-2-(4′-pyridyl)-3-(3′-cyanophenyl)benzo[*e*]indole) in the presence of $NaN_3$ (see Fig. 11). The precursor L ligand was chosen for the construction of the acentric because it contains two chiral centers (highly kink) and a cyano group which can be converted into the tetrazole functionality via the *in situ* R. Huisgen [3 + 2] cycloaddition reaction which was revisited by K.B. Sharpless [19].

X-ray crystallography shows that the local coordination geometry around the Cd(II) center is a slightly distorted octahedron (see Fig. 12). The Cd(II) metal center bonds to the four N atoms of the L ligands (two from the pyridyl rings and two from the tetrazole rings), and to two water molecules through the oxygen atoms. The four bonded N atoms are located in a plane that is equatorial with respect to each other while the two bonded O atoms are situated in axial positions to the plane. Each L acts as a bidentate linker that bridges two Cd centers. Each Cd center is bridged by four L ligands to result in an infinite Cd–Cd molecular box along the crystallographic *a* axis. Two adjacent Cd centers in this infinite molecular box form a 28-membered ring (Cd(NC9N3)2Cd) with four bridging L. Compound **7** displays a 1D $M_2L_2$ rhombohedral molecular square with an approximate dimension of $10.37 \times 6.64\ Å^2$. No interpenetration was found in this square. Furthermore, there are no open

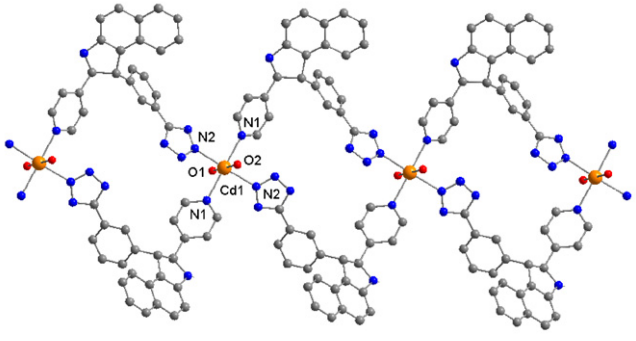


**Fig. 12.** 1D structure of **7** with $M_2L_2$ box [19].

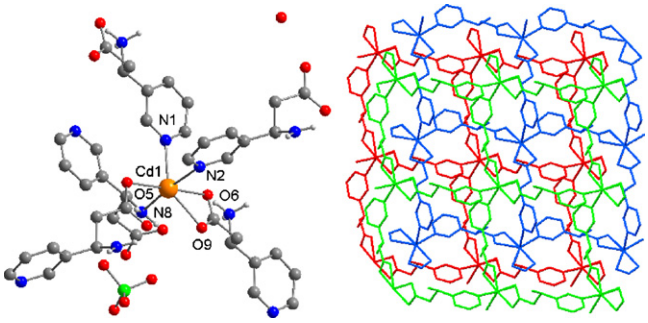


**Fig. 13.** Coordination of Cd center composed of four *rac*-Hpapa ligands in **8** and its 2-fold interpenetrating 3D framework with a (10, 3b) topology [20].

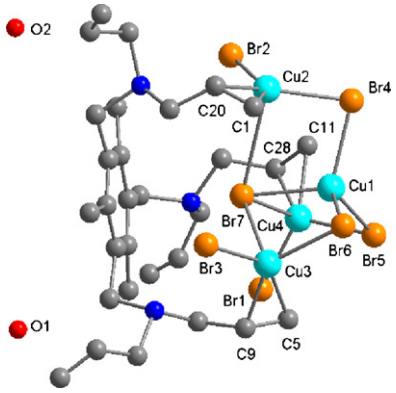


**Fig. 14.** Asymmetric unit of olefin-copper(I) coordination compound **9** in which three allyl groups of one olefin organic ligand coordinate to three independent copper(I) centers [21].

channels found in the packing state and the adjacent layers stacking mode can be seen as ABAB type in a staggered arrangement. The co-linear adjacent 1D chains align in the same direction with respect to each other that prevents the cancellation of the dipolar moments, probably due to many weak interactions (H-bond, π–π stacking, hydrophobic and hydrophilic as well as van der Waals interactions).

Since **7** adopts the acentric space group *Aba*2 (crystal class *mm*2 and point group $C_{2v}$), it should exhibit ferroelectricity in principle. Compound **7** shows moderate ferroelectric behavior with a weak electric hysteresis loop with $P_r$ of 0.12–0.28 μC cm$^{-2}$ and $E_c$ of 10 kV cm$^{-1}$.

### 3.2. *[Cd(rac-papa)(rac-Hpapa)]$ClO_4$·$H_2O$ (**8**)*

Another successful self-assembled example of acentric MOCP through supramolecular crystal engineering strategy is [Cd(*rac*-papa)(*rac*-Hpapa)]$ClO_4$·$H_2O$ (**8**) (*rac*-Hpapa = racemic 3-(3-pyridyl)-3-aminopropionic acid). It was obtained by a methanolothermal reaction of Cd$(ClO_4)_2$·6$H_2O$ with *rac*-Hpapa at 78 °C over a period of a week [20].

X-ray single crystal structural determination discloses that **8** is a complex 3D anionic network containing a unique cadmium atom and two unique bridging ligands. The connectivity of the network is perhaps most easily understood in terms of square-grid sheets that extend in the *ab* plane (see Fig. 13). The ligands that extend down the page (vertical ligands) are identical, but are different to the ligands that bridge Cd atoms across the page (horizontal ligands). For the vertical ligands, the primary amino groups are protonated, forming primary ammonium groups. This nitrogen atom and the non-coordinated carboxylate oxygen atom are involved in an intra-ligand hydrogen bond. There are two unique ligands which are chemically similar. The roles they play in the net connectivity are quite different, that is, one of the ligands connects to three cadmium centers and the other to two. Totally this topology can be attributed to 2-fold interpenetrating (10, 3b) net. Interestingly, there are extensive hydrogen bonds among protonated amino groups, perchlorate anions and water, as is the case in TGS.

Compound **8** crystallizes in the acentric space group *Cc*, corresponding to the polar point group *C*s. Experimental results indicate that **8** displays ferroelectric behavior with a clear electric hysteresis loop with a $P_r$ of 0.18–0.28 μC cm$^{-2}$ and an $E_c$ of 12 kV cm$^{-1}$. It is interesting to note that **8** contains protonated amino groups participating in extensive hydrogen bonding like that in TGS.

### 3.3. *[($H_3$TTT)($Cu_4Br_7$)]($H_2O$)$_2$ (**9**)*

A novel olefin-copper(I) organometallic compound [($H_3$TTT)($Cu_4Br_7$)]($H_2O$)$_2$ (**9**) was obtained via solvothermal treatment of the flexible olefin organic ligand TTT (TTT = *N*,*N*′,*N*″-(2,4,6-trimethyl-benzene-1,3,5-triyl)tris(methylene) tris(*N*-allylprop-2-en-1-amine) and CuBr in the presence of hydrobromide acid and methanol as solvent at 75 °C [21].

The crystal structure of compound **9** reveals that the nitrogen atoms in the olefin organic ligand are all protonated. The three allyl arms chelate to a [$Cu_4Br_7$]$^{3-}$ cluster to form a bowl-like discrete structure (see Fig. 14). In the asymmetric unit, there are four crystallographically different copper(I) centers: one taking a trigonal plane geometry and the other three taking a distorted tetrahedron geometry. Meanwhile, bromide atoms have three types of coordination modes, i.e., terminal, bidentate bridge, and tridentate bridge, to connect the copper(I) atoms together to form the [$Cu_4Br_7$]$^{3-}$ aggregate. There are strong hydrogen-bonding interactions among protonated nitrogen atoms, Br atoms and crystallized water, which result in the formation of 3D framework.

The induction of the flexible ligand leads the olefin-copper(I) organometallic compound **9** to crystallize in a chiral space group $P4_1$ (polar point group $C_4$), meaning a potential ferroelectric property. The measurements show typical electric hysteresis loops with a $P_r$ of *ca.* 0.2 μC cm$^{-2}$ and an $E_c$ of *ca.* 0.8 kV cm$^{-1}$.

### 3.4. *[($CH_3$)$_2$$NH_2$]Zn($HCOO$)$_3$ (**10**)*

Cheetham et al. studied the order–disorder antiferroelectric phase transition in a perovskite-type hybrid inorganic–organic framework [($CH_3$)$_2$$NH_2$]Zn($HCOO$)$_3$ (**10**). Compound **10** was synthesized in a reaction between zinc chloride and water in dimethylformamide (DMF). The formic acid and dimethyl ammonium cation as building blocks for **10** come from *in situ* hydrolysis of DMF [22].

Compound **10** crystallizes in a central space group $R\bar{3}c$ at 180 K, corresponding to the paraelectric phase. The $Zn^{2+}$ center is interconnected by deprotonated formic acid moieties to form a 3D framework (see Fig. 15). The coordination geometry of the six oxygen atoms around $Zn^{2+}$ is approximately octahedral. The dimethylamine cation locates in the voids of the framework of **10**. It is disordered with nitrogen apparently existing in three different possible positions, as a consequence of disordered hydrogen bonding between the hydrogen atoms of the $NH_2$ group and oxygen atoms from the formate framework (N···O = 2.9 Å).

A phase transition was evidenced by single crystal X-ray diffraction and synchrotron X-ray powder, consistent with ordering of the $NH_2$ hydrogen atoms. A dielectric anomaly, as expected for a perovskite, was found around 160 K with a clear hysteresis of about 10 K. The shape of the dielectric plot around 160 K furnishes clear evidence that **10** becomes antiferroelectric below 160 K on cooling. Compound **10** also falls into the category of high-dielectric constant material with an $\varepsilon_r$ value of 15. This type of electrical ordering asso-

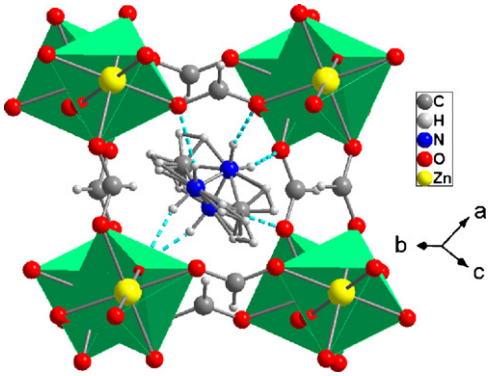


**Fig. 15.** Crystal structure of **10** [22].

ciated with an order–disorder phase transition is unprecedented in hybrid frameworks and opens up an exciting new direction in rational synthetic strategies to create extended hybrid networks for applications in ferroic-related fields.

### 3.5. $Rb^{I}_{0.82}Mn^{II}_{0.20}Mn^{III}_{0.80}[Fe^{II}(CN)_6]_{0.80}\,[Fe^{III}(CN)_6]_{0.14}\cdot H_2O$ (**11**)

Magnetism and ferroelectricity are essential to many forms of current technology, and the quest for multiferroic materials, where these two phenomena are intimately coupled, is of great technological and fundamental importance [23]. Despite their usefulness, magnetic ferroelectrics are rare in nature and most of them are antiferromagnets with small responses to external magnetic field because ferroelectricity and magnetism tend to be mutually exclusive and interact weakly with each other when they coexist.

A successful MOCP with the coexistence of ferroelectricity and ferromagnetism in $Rb^{I}_{0.82}Mn^{II}_{0.20}Mn^{III}_{0.80}[Fe^{II}(CN)_6]_{0.80}[Fe^{III}(CN)_6]_{0.14}\cdot H_2O$ (**11**) was reported by Ohkoshi et al. at low temperature [24]. Variable-temperature XRD measurements reveal that **11** displays phase transition at high temperature (276 K, a centrosymmetric space group *F*43*m*) and low temperature (184 K, an acentric space group *F*222 belonging to non-polar point group $D_2$). The crystal structure may resemble that of Prussian blue (see Fig. 16).

The magnetization *vs.* temperature plots of the low-temperature phase show ferromagnetism with a Curie temperature of 11 K. The *P*–*E* plot for the low-temperature phase at 77 K, when applying a field up to 100 kV cm$^{-1}$, shows an electric hysteresis loop with a $P_r$ of 0.041 μC cm$^{-2}$ and an $E_c$ of 17.5 kV cm$^{-1}$. The ferroelectricity may be related to mixing of $Fe^{II}$, $Fe^{III}$, Fe vacancy, $Mn^{II}$, and Jahn–Teller-distorted $Mn^{III}$. One of the possible mechanisms of the ferroelectricity may be explained as follows. In **11**, a multimetallic Prussian blue analogue, a local electric dipole moment is created because of an Fe vacancy. In addition, the difference in ionic radii among four metal ions and $Mn^{III}$ Jahn–Teller distortion enhance the local structural distortion, for example, the deviation of M–CN–M′ linkages from a 180° configuration. Probably, in such a deviated structure, polarization will be induced by the applied electric field, and the polarization can be held by the structural flexibility of the cyano-bridged 3D network.

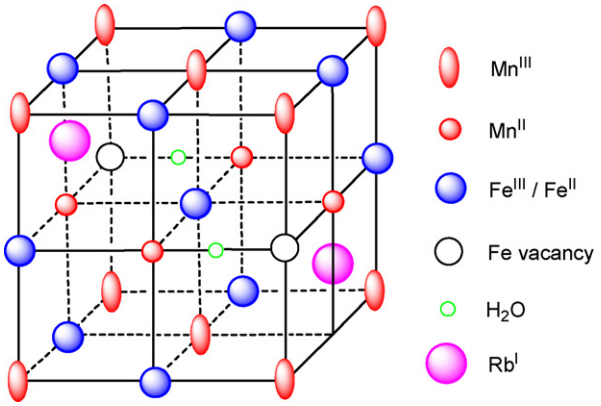


**Fig. 16.** A schematic illustration of the molecular structure of the Prussian blue analogue **11** [24].

### 3.6. $Cu^{II}_2[Mo^{IV}(CN)_8]\cdot 8H_2O$ (**12**)

Another Prussian blue analogue, $Cu^{II}_2[Mo^{IV}(CN)_8]\cdot 8H_2O$ (**12**), was prepared from a mixing of copper salt and $K_4[Mo^{IV}(CN)_8]$. This compound takes a 3D structure where the Cu ions connect with the Mo ions through the N atoms of the CN bridges, displaying paramagnetism [25].

In the ferroelectric phase, the crystal structure is supposed to take a polar group of $C_{\infty v}$ after application of an electric field. The *P vs. E* curve of the compound at 145 K shows a hysteresis loop with a $P_r$ of 0.036 μC cm$^{-2}$ and an $E_c$ of 5.5 kV cm$^{-1}$. This compound has a freezing point for the fixation of hydrogen bonding at 150 K, around which an enhancement in the ferroelectricity and an increase in the dielectric constant are observed. On the basis of the results of ferroelectric, dielectric, and structural measurements, the ferroelectricity of this system is classified into amorphous ferroelectrics, i.e., the electric poling effect induces an electric polarization. The electric polarization is maintained by the structural local disorder of hydrogen bonding and the 3D CN network.

### 3.7. $[Mn_3(HCOO)_6](CH_3OH)$ (**13**)

Another possible ferroelectric and ferrimagnetic MOCP with structural phase transition is the porous molecular crystal $[Mn_3(HCOO)_6](CH_3OH)$ (**13**), where $CH_3OH$ is guest molecule (see Fig. 17) [26].

Compound **13** is a porous magnet showing a ferrimagnetic transition at $T_c$ = 8.5 K. Low-temperature X-ray structural determination

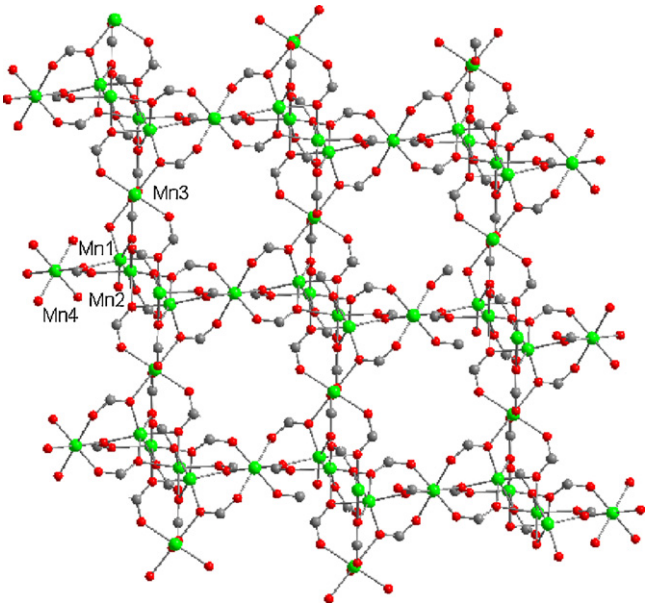


**Fig. 17.** Porous 3D molecular structure of **13** without showing the guest molecules [26].

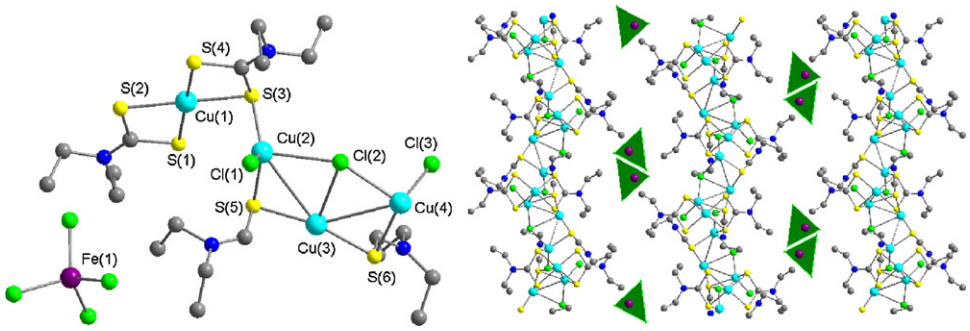


**Fig. 18.** Asymmetric unit of **14** and its 2D laminar view [27].

shows that its space group may be an acentric one belonging to ferroectricity active point group. Ferroelectric test shows that **13** has ferroelectric order below 165 K confirmed by its dielectric anomaly (a change of dielectric constant near Curie–Weiss temperature) and differential scanning calorimetry (DSC) at low temperature. The ferroelectricity is considered to come mainly from the guest molecules, suggesting the important role of the host–guest interaction.

### 3.8. $[Cu^{I}_4Cu^{II}(Et_2dtc)_2][Cu^{II}(Et_2dtc)_2]_2(FeCl_4)$ (**14**)

A mixed-valence coordination polymer, $[Cu^{I}_4Cu^{II}(Et_2dtc)_2][Cu^{II}(Et_2dtc)_2]_2(FeCl_4)$ ($Et_2dtc^-$ = diethyldithiocarbamate) (**14**), was obtained by a reaction of a $CHCl_3$ solution of $Fe(Et_2dtc)_3$ and an acetone solution of $CuCl_2{\cdot}2H_2O$ [27].

A single crystal X-ray analysis reveals that the asymmetric unit of **14** consists of a pentanuclear copper fragment $Cu_5(Et_2dtc)_2Cl_3$, two bridging mononuclear copper units $Cu(Et_2dtc)_2$ and a counteranion $FeCl_4^-$ (see Fig. 18). The magnetic measurement of **14** suggests weak interactions ($\theta = -1.03$ K) between the unpaired electrons of the Cu(II) ions. At 260 and 300 K, the ferroelectric measurements clearly show that there are hysteresis loops. The ferroelectric behavior was also confirmed by a relatively large dielectric constant ($\varepsilon_r \approx 6.1$) observed in **14** with a 2D ferroelectric structural order. However, unfortunately, crystal structural determination at room temperature shows that **14** has a centrosymmetric space group (*Pnma*) which does not agree with its ferroelectric behavior, probably due to the presence of $Fe^{III}$ ion.

### 3.9. $[Cu(4,4'\text{-}H_2bpz)Br]{\cdot}0.5H_2O$ (**15**)

$[Cu(4,4'\text{-}H_2bpz)Br]{\cdot}0.5H_2O$ (**15**, 4,4′-$H_2$bpz = 3,3′,5,5′-tetramethyl-4,4′-bipyrazole) was synthesized by the reaction of CuBr, 4,4′-$H_2$bpz, $CH_3CH_2OH$ and $H_2O$ under hydrothermal conditions [28].

Single crystal X-ray crystallographic analysis reveals that MOCP **15** has a non-interpenetrating, 3D porous framework constructed from copper ions and $\mu_2$-4,4′-$H_2$bpz ligands. The asymmetric unit of **15** contains half a 4,4′-$H_2$bpz ligand, half a copper ion and half a bromine ion (see Fig. 19). The Cu1 atom is coordinated by two Br1 and two N1 atoms from two different 4,4′-$H_2$bpz ligands to form a distorted tetrahedral geometry, which can be considered as a four-connected node to form a diamond-net structure. The framework is based on inorganic columns of the unusual castellated $(CuBr)_\infty$ chains. Each castellated chain is linked to four neighboring castellated chains by 4,4′-$H_2$bpz molecules to form a 3D porous framework, leading to a structure with a hexagonal array of channels.

Experimental results indicate that there is an electric hysteresis loop that is a typical ferroelectric feature with a $P_r$ of *ca.* 0.027 μC cm$^{-2}$ and an $E_c$ of *ca.* 1.88 kV cm$^{-1}$.

### 3.10. $[Ag_8(L)_4](NO_3)_8{\cdot}4H_2O$ (**16**)

A novel 3D metal-organic framework $[Ag_8(L)_4](NO_3)_8{\cdot}4H_2O$ (**16**) has been solvothermally synthesized by self-assembly of a new tetradentate imidazolate ligand L (L = bis(3,5-bis((1*H*-imidazol-1-yl)methyl)-2,4,6-trimethylphenyl)methane) and silver(I) salt [29].

X-ray crystallography of MOCP **16** reveals that each Ag(I) center takes a linear geometry by coordinating to two N atoms from different L (see Fig. 20). Each single net comprises linked Ag–L meso-helices. The distance between Ag2 and Ag2B is 3.044(1) Å, which is markedly shorter than the sum of the *van der Waals* radii of two silver atoms (3.44 Å), indicating a significant intramolecular Ag···Ag interaction. A single 3D network of MOCP **16** consists of Ag1–L meso-helices bridged by L and Ag2 atoms, exhibiting vase-like nanometer-sized channels (*ca.* 16.3 × 15.4 Å$^2$) along the [0 1 3] axis. The lattice is composed of rare 3-fold interpenetrating $4.14^2$ nets.

The compound crystallizes in a noncentrosymmetric space group *Fdd*2 associated with the polar point group $C_{2v}$. Its possible ferroelectric behavior has been studied, showing a hysteresis loop with a $P_r$ of 0.036 μC cm$^{-2}$ and an $E_c$ of 5.5 kV cm$^{-1}$.

### 3.11. $[Cd(Htrtr)_2]$ (**17**)

The reaction of $Cd(ClO_4)_2{\cdot}6H_2O$ with Htrtr (Htrtr = 3-(1,2,4-triazole-4-yl)-1*H*-1,2,4-triazole) under solvothermal conditions yielded a novel 3D MOCP $[Cd(Htrtr)_2]$ (**17**) [30].

Compound **17** crystallizes in the orthorhombic space group *Fdd*2 (polar point group $C_{2v}$). It adopts a 3D (3,6)-connected topological architecture. The local coordination geometry around the Cd(II) center is a slightly distorted octahedron (see Fig. 21). The Cd(II) metal center bonds to six N atoms from six L ligands while each ligand donates three N atoms to coordinate with three Cd(II) centers. The noncentrosymmetric polar packing arrangement results

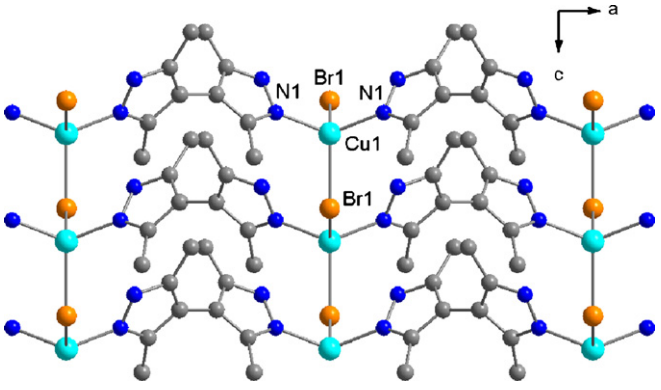


**Fig. 19.** 2D laminar view of **15** [28].

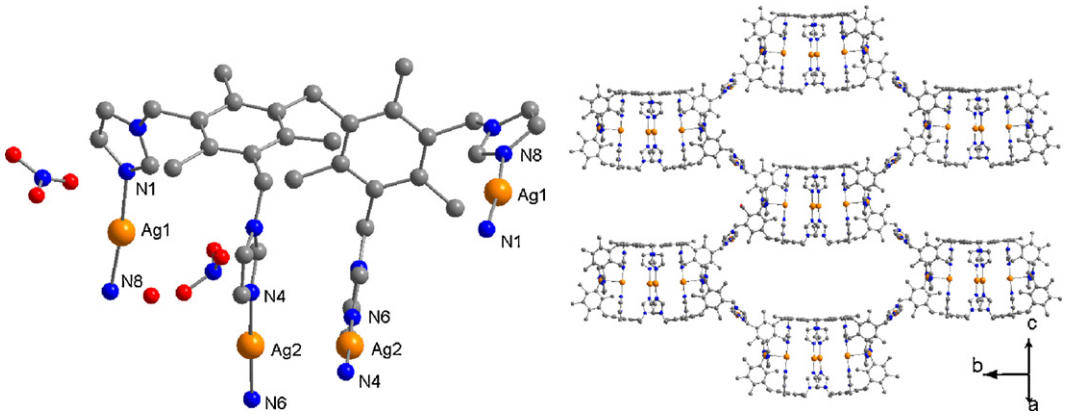


**Fig. 20.** Asymmetric unit of **16** and its 2D laminar view [29].

in a ferroelectric property with a $P_r$ of 0.004 μC cm$^{-2}$ and an $E_c$ of 2.5 kV cm$^{-1}$.

Although phase transition (cases **10**–**14**) will change the solid state structure from high symmetry to low symmetric acentric space group where ferroelectric behavior occurs, it is worth noting that the ferroelectric behavior is still weak. However, cases **7** and **8** tell us that the acentric MOCP with magnetism may be constructed through multi-chiral centers ligand (highly kink) as building blocks combining with transition metals.

## 4. Homochiral MOCPs constructed by optical organic ligand

### *4.1. Olefin-Cu(I) MOCPs (**18a**–**18e**)*

#### *4.1.1. [(H$_2$Q)$_2$Cu$_5$Cl$_9$] (**18a**)*

The first KDP-like 1D homochiral MOCP [(H$_2$Q)$_2$Cu$_5$Cl$_9$] (**18a**) (H$_2$Q = bi-protonated quinine) was obtained by the reaction of CuCl, quinine, and HCl in methanol under solvothermal conditions at 60–70 °C [31]. The crystal structure reveals that **18a** has a chiral space group *C*2 (polar point group $C_2$) with an anionic 1D polymer of composition [Cu$_5$Cl$_9^{4-}$]$_n$. The polymer contains Cu$_4$Cl$_6^{2-}$ adamantane-type aggregates that are linked to two identical units by CuCl$_3^{2-}$ bridges. The CuCl$_3^{2-}$ bridge is disordered around a 2-fold axis. There are three unique Cu atoms, two of which are in trigonal coordination geometries and the third is in a tetrahedral environment. The anionic charge of this highly unusual Cu(I)–Cl polymer is balanced by diprotonated quinine cations. The protons that are bound to the nitrogen atoms of the quinoline and quinuclidine rings participate in hydrogen bonds with chlorine atoms belonging to two Cu$_4$Cl$_6$ aggregates which are each part of two separate polymeric chains. As a consequence of the extensive coordination and hydrogen bonds, a homochiral 3D network is produced (see Fig. 22).

Ferroelectric measurement confirms that **18a** is a typical ferroelectric with a clear hysteresis loop with a $P_r$ of 0.28 μC cm$^{-2}$ and an $E_c$ of 16 kV cm$^{-1}$. The similarity found in **18a** and KDP is interesting that both form 3D networks with H-bond. Furthermore, although **18a** does not form a diamond-type net like KDP, it does possess adamantane-type units (in the anionic polymer), which are a characteristic structural feature of diamond nets.

#### *4.1.2. [(H$_2$Q)$_2$Cu$_3$Br$_7$](H$_2$O) (**18b**)*

To investigate the anion influence on structure motif, a similar reaction of CuBr with quinine (Q) in the presence of HCl was carried out. [(H$_2$Q)$_2$Cu$_3$Br$_7$](H$_2$O) (**18b**) was obtained, in which diprotonated quinines play a similar role and serve as countercations for anionic [Cu$_3$Br$_7^{4-}$]$_n$ chains [31].

The Cu$^{I}$ centers in this structure have a distorted tetrahedral geometry coordinated with bridging and terminal bromide ions. As is the case in **18a**, there are significant interactions between the H atoms on the N atoms of the quinoline and quinuclidine rings and

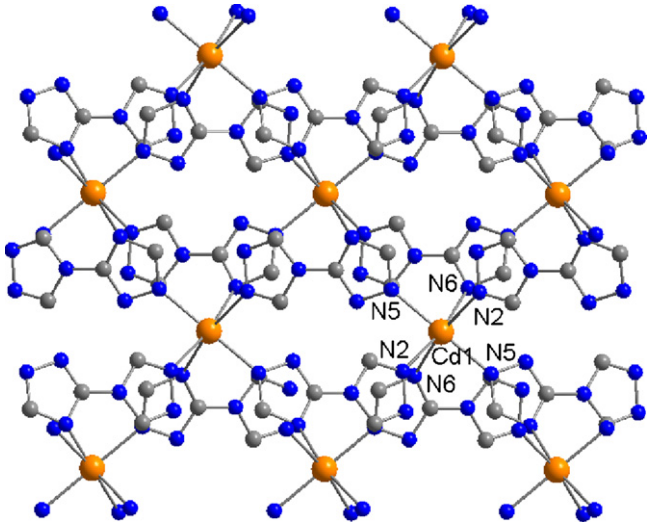


**Fig. 21.** 2D laminar view of **17** [30].

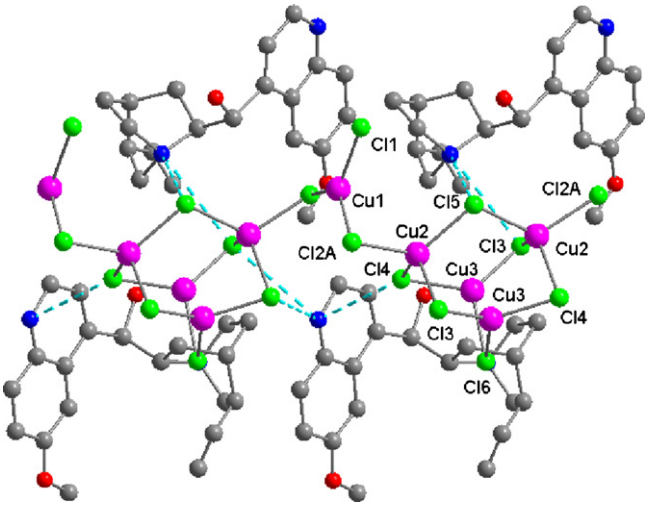


**Fig. 22.** 1D polymeric diamond-like structure (Cu$_n$Cl$_n$ forming 1D chain with diamond net as connecting node, not shown here and see original paper) and H-bond in **18a** [31].

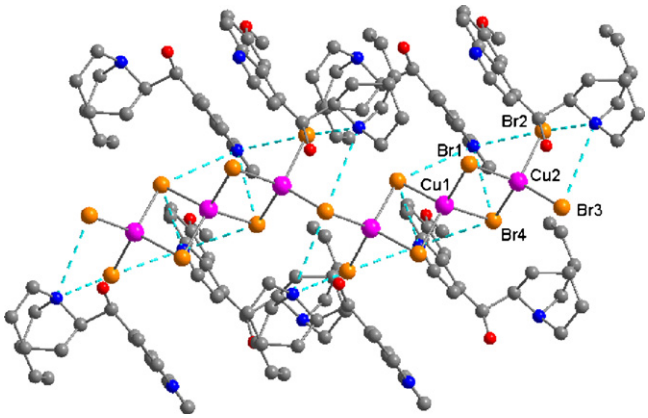


**Fig. 23.** 1D polymeric diamond-like structure and H-bond in **18b** [31].

Br atoms of the $Cu_3Br_7^{4-}$ polymer, resulting in the formation of a 3D homochiral network (see Fig. 23).

Similarly, **18b** has a chiral space group *C*2. Ferroelectric measurement shows that it is ferroelectricity active with a $P_r$ of 0.14 μC cm$^{-2}$ and an $E_c$ of 12 kV cm$^{-1}$.

*4.1.3. [$Cu_8X_{10}$(H-Q)$_2$] (**18c**, X = Cl; **18d**, X = Br)*

The first organometallic ferroelectric MOCP is [$Cu_8Cl_{10}$(H-Q)$_2$] (**18c**). It was prepared by solvothermal reaction of Q with CuCl in the presence of HCl [32]. The crystal structure of **18c** reveals that the Q is only monoprotonated and acts as a bridging ligand (see Fig. 24). In the structure, a 2-fold axis passes through an irregular discrete $[Cu_8Cl_{10}]^{2-}$ aggregate. The terminal copper center (Cu1) coordinates with a quinoline nitrogen of one H-Q, a C=C moiety of another H-Q, and a bridging chloride ion. The remaining copper centers, Cu2, Cu3, and Cu4, are in approximately trigonal, pyramidal, and linear coordination geometries, respectively, surrounded by chloride ions. An unusual feature of this anion is the sharp kink at Cl6 with a Cu2–Cl6–Cu4 angle of 74.20(8)°. This brings Cu2 and Cu4 into a close contact (2.700(2) Å) and allows Cl5 to form a weak interaction with Cu3 (2.727(3) Å). Each $[Cu_8Cl_{10}]^{2-}$ aggregate is linked to other four equivalent aggregates through the bridging H-Qs, resulting in a 2D-layered network. The arrangement of adjacent layers of the 2D network is AA type packing.

Compound **18c** crystallizes in space group *C*2, and its ferroelectric property is expected. The experimental results clearly indicated

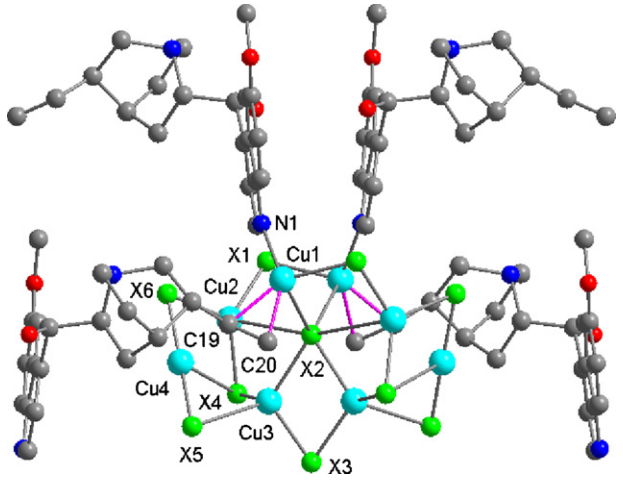


**Fig. 24.** An asymmetric unit representation with $Cu_8X_{10}$ cluster as supporter in **18c** and **18d** [32].

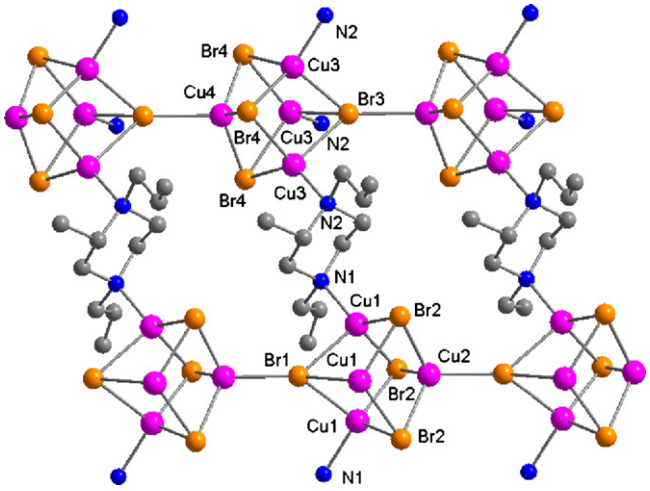


**Fig. 25.** 2D structure of **18e** [33].

the electric hysteresis loop with a $P_r$ of *ca.* 0.12 μC cm$^{-2}$ and an $E_c$ of 5.0 kV cm$^{-1}$.

An analogue [$Cu_8Br_{10}$(H-Q)$_2$] (**18d**) also crystallizes in a chiral space group *C*2, and is basically isostructural to **18c**. But its hysteresis loop cannot be measured due to a large current leakage.

*4.1.4. [(DAMP)$_3$($Cu_4Br_4$)$_2$($H_2O$)$_3$] (**18e**)*

The methanolothermal reaction of (*S*)-1,4-diallyl-2-methylpiperazine (DAMP) with an excess CuBr affords a novel homochiral 3D framework [(DAMP)$_3$($Cu_4Br_4$)$_2$($H_2O$)$_3$] (**18e**) [33].

The X-ray crystal structural determination of **18e** reveals that the geometry of the Cu center is a slightly distorted tetrahedron in which three $\mu_3$-Br atoms and one N atom from an (*S*)-DAMP ligand form four coordination bonds with the Cu1 center while three $\mu_3$-Br atoms and one $\mu_4$-Br atom form four coordination bonds with the Cu2 center, as shown in Fig. 25. The $\mu_4$-Br atom connects two $Cu_4Br_4$ cubanes to result in the formation of a 1D chain. A 3D framework is formed owing to the connections of the organic ligand DAMP and the $\mu_4$-Br atoms with the Cu atoms in the three directions.

Compound **18e** crystallizes in a chiral space group *P*3 belonging to a polar point group $C_3$. Preliminary studies indicate that it displays ferroelectric behavior with a $P_r$ of *ca.* 1.4–2.5 μC cm$^{-2}$ and an $E_c$ of *ca.* 0.65–1.0 kV cm$^{-1}$.

*4.2. [(HQA)($ZnCl_2$)(2.5$H_2O$)] (**19**)*

The ligand quitenine (6-methoxyl-(8*S*,9*R*)-cinchonan-9-ol-3-carboxylic acid, HQA) was prepared by oxidizing Q by $KMnO_4$ at low temperature. 1D chain homochiral [(HQA)($ZnCl_2$)(2.5$H_2O$)] (**19**) containing HQA as building block was obtained by the reaction of $ZnCl_2$ with HQA [34].

X-ray crystal structure analysis of **19** reveals that there are two crystallographically independent Zn centers whose geometry is a slightly distorted tetrahedron defined by two Cl anions and the N atom of quinoline ring along with an oxygen atom from the carboxylate group (see Fig. 26). Thus, each quitenine ligand acts as a bidentate spacer that links two Zn centers to a 1D chain coordination polymer. To balance the charges in **19**, the N atom of the quinuclidine ring is protonated, forming a zwitterionic moiety similar to natural α-amino acids (HQA being a β-amino acid). The packing mode reveals that each wave-like chain adopts AA typed packing, preventing the cancellation of the dipolar moments.

The space group *P*1 is associated with the point group $C_1$, required for ferroelectric behavior. The experimental results reveal

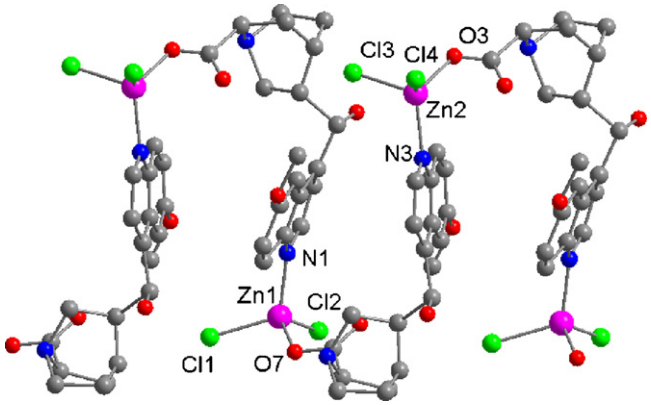


**Fig. 26.** 1D wave-like chain structure in **19** [34].

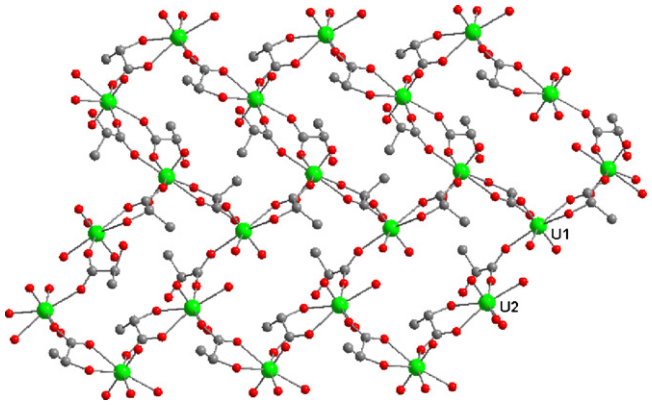


**Fig. 28.** 2D network of **21** viewed along the *a* axis [36].

that **19** is ferroelectrically active with a $P_r$ of 0.04 μC cm$^{-2}$ and an $E_c$ of 25 kV cm$^{-1}$. Interestingly, the measurement of dielectric loss clearly indicates that there is a relaxation process with an activity energy $E_a$ = 0.94 eV and relaxation time $\tau = 1.6 \times 10^{-5}$ s. Combined with its large dielectric constant ($\varepsilon_0$ = 37.3), **19** may take a chain micro-vibration to result in an overall chain–chain dipolar relaxation process to induce ferroelectric behavior.

### 4.3. *[Zn(HQA)Br$_2$(X$_2$O)$_3$] (**20a**, X = H; **20b**, X = D)*

1D chain homochiral [Zn(HQA)Br$_2$(H$_2$O)$_3$] (**20a**) and [Zn(HQA)Br$_2$(D$_2$O)$_3$] (**20b**) were prepared by thermal treatment of HQA with ZnBr$_2$ in either H$_2$O or D$_2$O and 2-butanol at 70 °C for 1–2 days [35].

Crystal structural determinations of **20a** and **20b** reveal that both of them are isostructural and crystallize in a chiral space group *C*2 belonging to polar point group $C_2$. The N atom of the quinuclidine ring is protonated. This implies that the HQA ligand in **20a** and **20b** exists in a zwitterionic form, which would not be surprising given that the ligand is a β-amino acid. X-ray single crystal structural determination of **20a** reveals that the local coordination geometry around the Zn center is a slightly distorted tetrahedron composed of two terminal Br anions, an oxygen atom from the carboxylate group and a N atom from the quinoline ring (see Fig. 27). Each HQA acts as a bidentate spacer that links two Zn centers together to furnish a 1D wave-like chain.

The dipolar moment along each chain can be considered with the negative and positive charges sitting on the oxygen atom of carboxylate group and N atom of quinuclidine ring, or Cl and Zn atoms, respectively. This results in each chain dipolar moment always moving in the same direction and strengthening of the total dipolar moment within the chains, which cannot therefore be cancelled. The presence of numerous H-bonding interactions in **20a** results in the formation of an H-bonded 3D framework. Compounds **20a** and **20b** are isostructural with respect to each other. Pellets of powdered samples of **20a** and **20b** clearly show that both MOCPs exhibit typical ferroelectric behavior (hysteresis loop), and display $P_r$ of *ca.* 0.16 μC cm$^{-2}$ for **20a** and 0.17 μC cm$^{-2}$ for **20b**.

There is a slight ferroelectric DEF (with an increase in the $P_s$ value of 13%) [(0.34–0.30)/0.30] detected on going from **20a** to **20b**. However, by assuming one dipole in the unit cell ($Z$ = 2) (the density of dipoles, $N_1 = Z/V_{cell} = 1.5657 \times 10^{27}$ m$^{-3}$ for **13a**), it should be noted that the cubic moment $\mu_s = P_s/N_1 = 1.916 \times 10^{-30}$ C m ≈ 0.57 Debye (calculated from the saturated polarization $P_s$ (0.30 μC cm$^{-2}$)). Similarly, $N_2$ is equal to $Z/V_{cell} = 1.568 \times 10^{27}$ m$^{-3}$ for **20b** and $\mu_s$ is equal to $P_s/N_2 = 2.168 \times 10^{-30}$ C m ≈ 0.65 Debye, which is slightly larger than that of **20a**. These ferroelectric features are further confirmed by their large dielectric constants (362 and 485).

### 4.4. *Uranyl-bis[(S)-lactate] (**21**)*

A 2D laminar ferroelectric MOCP is uranyl-bis[(*S*)-lactate] (**21**) obtained from a *in situ* hydrothermal reaction of $UO_2(NO_3)_2$ with ethyl (*S*)-lactate [36]. X-ray crystal structural determination reveals that the local coordination geometry around each U atom center in **21** is a distorted pentagonal bipyramid (see Fig. 28). However, there are two crystallographically different U centers and three kinds of lactate ligands: one serves as a bidentate ligand to chelate one U atom using two O atoms from one carboxylate and one hydroxy group; the second lactate ligand acts as a bidentate bridge to link two U atoms using one carboxylate group; the last lactate ligand is a monodentate terminal group with coordination of its carboxylate to one U atom to form a 2D brick-wall type grid network. The relationship between two layers is an ABAB-type stack and no interpenetration is found in **21**.

It crystallizes in the chiral space group $P2_1$ belonging to the crystal classes 2 (polar point group). The experimental results show that there is a weak electric hysteresis loop with a $P_r$ of

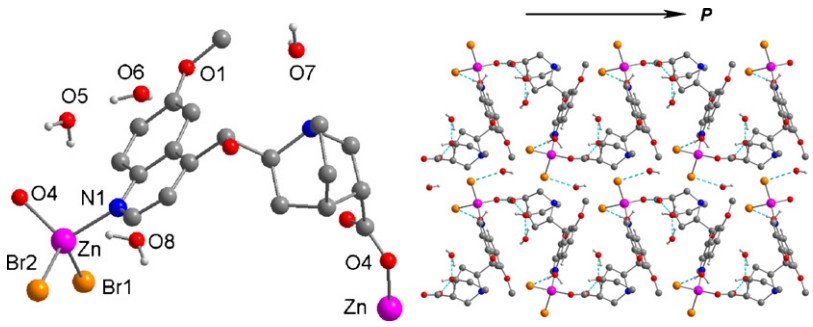


**Fig. 27.** Asymmetric unit in **20a** and **20b** and their 3D framework with same direction alignment [35].

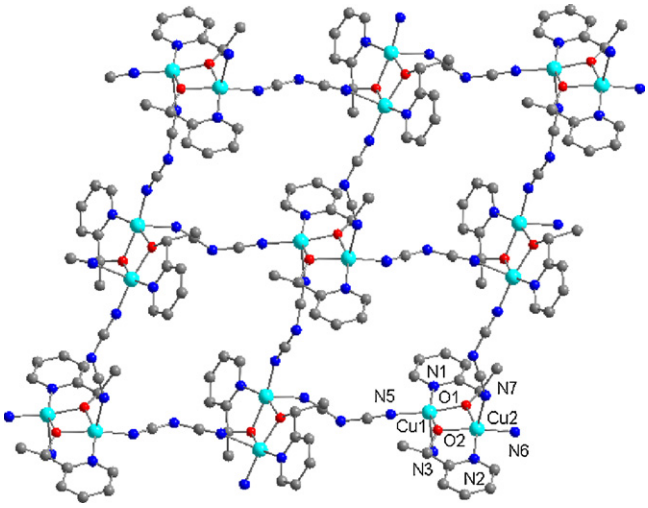


**Fig. 29.** 2D laminar view in MOCP **22** [37].

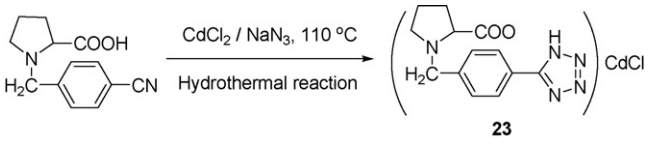


**Fig. 30.** Synthesis of **23** [38].

0.12 μC cm$^{-2}$ and an $E_c$ of 5 kV cm$^{-1}$. Maybe the H-bond and layered structure are responsible for the ferroelectric behavior in **21**.

### 4.5. [Cu((R)-mpm)(dca)] (**22**)

To explore possible multiferroic MOCP, one homochiral [Cu((*R*)-mpm)(dca)] (**22**) ((*R*)-mpm = (*R*)-α-methyl-2-pyridinemethanol, dca = dicyanamide) was prepared by the reaction of (*R*)-mpm, $Cu(OAc)_2{\cdot}H_2O$, and Na(dca) in a 1:1:1 molar ratio in a methanol/water mixture at room temperature [37].

X-ray crystal structural determination reveals that **22** crystallizes in a chiral space group ($P2_1$). The local coordination geometry around $Cu^{II}$ ion is a distorted square-pyramidal: the two apical positions occupied by the two N atoms of two dca bridges and the equatorial plane occupied by two O atoms and one N atom of pyridyl ring (see Fig. 29).

Magnetic measurement shows that **22** displays strong antiferromagnetic couplings between spin centers. Meanwhile, ferroelectric measurement indicates that a typical hysteresis loop with a $P_r$ of 0.001 μC cm$^{-2}$ was found to confirm the presence of ferroelectricity in **22**.

### 4.6. [CdCl(H-TBP)] (**23**)

3D acentric [CdCl(H-TBP)] (**23**) (H-TBP = *N*-(4-(1*H*-tetrazol-5-yl)benzyl)proline) was prepared by the *in situ* hydrothermal [3 + 2] cycloaddition reaction of *N*-(4-cyanobenzyl)-(*S*)-proline with $NaN_3$ in the presence of $CdCl_2$ as Lewis acid catalyst (see Fig. 30) [38]. Due to high temperature, the racemization occurred during the in-synthesis of H-TBP.

X-ray single crystal determination discloses that **23** crystallizes in an acentric space group *Cc*. The Cd center sits in a slightly distorted octahedron that consists of three N atoms from two tetrazoyl groups and a pyrrolidinyl group, and a terminal Cl atom as well as two O atoms from two carboxylate groups (see Fig. 31). Each H-TBP ligand acts as a pentadentate bridging linker that connects five Cd atoms to form the 3D framework. Furthermore, an O atom from the carboxylate group of the H-TBP ligand binds to a Cd center that is also linked to a N atom from the pyrrolidinyl ring to give a stable five-membered ring. A second five-membered ring is found along the Cd–N–N–Cd–O bonding sequence with the μ-O atom from the H-TBP carboxylate group connecting two Cd ions that are also linked together via two N atoms from the tetrazoyl group.

The ferroelectric behavior of **23** was examined, finding that there is an electric hysteresis loop in **23** with a $P_r$ of *ca.* 0.38 μC cm$^{-2}$ and an $E_c$ of *ca.* 2.10 kV cm$^{-1}$. To evaluate the possible mechanism of ferroelectric behavior, the dielectric loss experiments were performed. The results indicate a relaxation process occurring in **23** with an activity energy of 1.96 eV and relaxation time of $1.60 \times 10^{-5.5}$ s, suggesting that its ferroelectric behavior is most likely relaxation-typed. The relaxation maybe originates from dipolar Cd–Cl bond vibration or the displacement of the proton on the tetrazoyl group.

### 4.7. [Cd(Imazethapyr)$_2$] (**24**)

Hydrothermal reaction of H-Imazethapyr (2-(4,5-dihydro-4-methyl-4-(1-methylethyl)-5-oxo-1*H*-imidazol-2-yl)-5-ethyl-3-pyridinecarboxylic acid, racemic) with $Cd(ClO_4)_2{\cdot}6H_2O$ at 110 °C offers MOCP Cd(Imazethapyr)$_2$ (**24**) [39]. The 5-oxo-1*H*-imidazole ring remains unchanged, so that Imazethapyr still is a chiral building block.

X-ray crystal structure determination of **24** reveals that the local coordination environment around the Cd ion adopts slightly distorted octahedron geometry. Each Imazethapyr ion links two Cd ions through one of the two O atoms of the carboxylate moiety and two N atoms of pyridyl and oxo-imidazole rings to chelate a Cd ion with a stable chelating ring (see Fig. 32). Interestingly, each Cd ions links four different Imazethapyr ions at four different directions to result in the formation of three-dimensional condensed framework. Each Imazethapyr ions acts as a linear link to connect two Cd centers while each Cd centers needs four such linear links to result in the formation of 3D diamond-like framework.

Compound **24** crystallizes in an acentric space group *Fdd*2, a polar space group required for ferroelectric behavior. Experimental results indicate that **24** displays ferroelectric behavior with

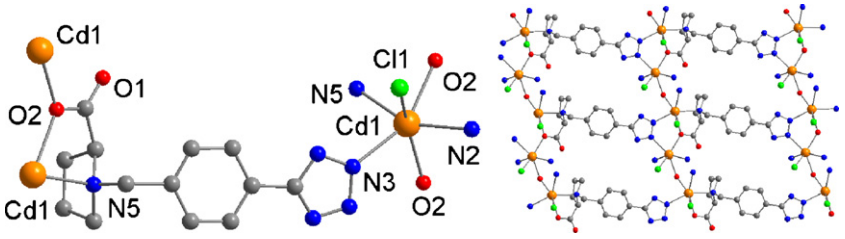


**Fig. 31.** Asymmetric unit view and 2D square-like net framework in **23** [38].

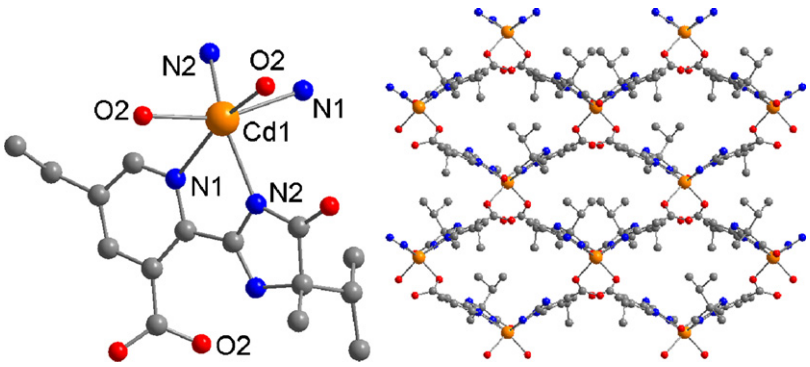


**Fig. 32.** Asymmetric unit view and 3D framework in **24** [39].

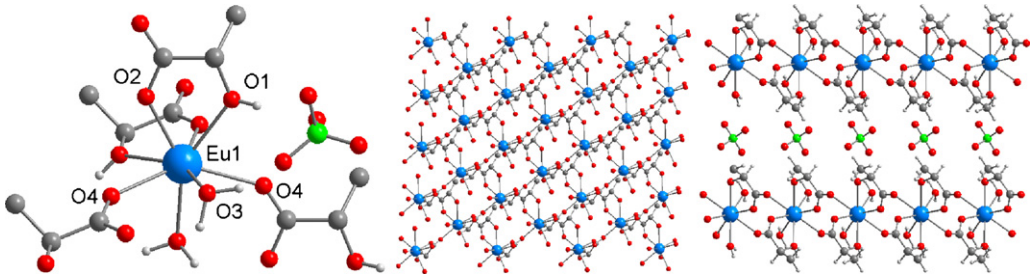


**Fig. 33.** Asymmetric unit view, 2D laminar and 3D homochiral framework in **25** [40].

a $P_r$ of *ca.* 0.006 μC cm$^{-2}$ and an $E_c$ of *ca.* 0.9–1.1 kV cm$^{-1}$. So it is a good potential ferroelectric material. Normally, ferroelectricity active compound should be piezoelectric active one because piezoelectric compounds only need to possess noncentrosymmetric structures. Our preliminary result indicates that **24** displays a $d_{33}$ value of *ca.* 60.1 pC N$^{-1}$.

### 4.8. *[Eu(Lac)$_2$(X$_2$O)$_2$](ClO$_4$) (**25a**, X = H; **25b**, X = D)*

Hydrothermal reaction of *L*-ethyl lactate (Lac-Et) with Eu(ClO$_4$)$_3$·6H$_2$O gives colorless block crystals of [Eu(Lac)$_2$(X$_2$O)$_2$](ClO$_4$) (**25a**, X = H; **25b**, X = D) [40].

X-ray crystal structure determination of MOCPs **25a** and **25b** reveal that both compounds possess a two-dimensional laminar homochiral framework (see Fig. 33). The local coordination environment around the Eu ion displays a slightly distorted square antiprism or dodecahedron with six oxygen atoms from four different lactate ions and two H$_2$O molecules (or D$_2$O) to complete the eight-coordination mode. A cationic laminar layer of [Eu(Lac)$_2$(X$_2$O)$_2$]$^+$ (X = H or D) acts as the sides of a sandwich to intercalate perchlorate ions, resulting in the formation 3D framework through hydrogen bonds.

Both compounds display a giant dielectric anisotropy approximately exceeding 100 and large isotopic effect with about 54% enhancement along the *a* axis. Their ferroelectric features further confirm this respect, showing a $P_r$ of *ca.* 0.025 μC cm$^{-2}$ and an $E_c$ of around 0.15 kV cm$^{-1}$ for **25a** and a $P_r$ of *ca.* 0.09 μC cm$^{-2}$ and an $E_c$ of *ca.* 0.24 kV cm$^{-1}$ for **25b**. Thus, deuteration effect of $P_r$ of **25b** is 3.6 times larger than that of non-deuterated **25a**. This work provides an insight in the search for highly anisotropic dielectrics. In generally, the laminar and homochiral MOCP will display large permittivity anisotropies.

### 4.9. *[(Lig)$_2$Tb(X$_2$O)$_2$](ClO$_4$) (**26a**, X = H; **26b**, X = D)*

The hydrothermal reaction of (*L*)-ethyl lactate (Lig-Et) with Tb(ClO$_4$)$_3$·6H$_2$O gives colorless block [(Lig)$_2$Tb(X$_2$O)$_2$](ClO$_4$) (**26a**, X = H; **26b**, X = D) [41].

X-ray crystal structure determination of **26** shows that the local coordination environment around the Tb ion is a slightly distorted square antiprism or dodecahedron, where six O atoms come from four different lactate ions while two water molecules completed the eight-coordination mode (see Fig. 34). Thus, each lactate ion links two Tb ions using one of the two O atoms of carboxylate and hydroxy groups to chelate the Tb ion while the other O atom of carboxylate bridges another Tb ion to result in the formation of a 2D-layered framework. The cationic laminar layers Tb(Lig)$_2$ are then intercalated by perchlorate ions to form a 3D framework through hydrogen bonds. Magnetic measurement seemingly indicates ferromagnetic coupling between the Tb$^{III}$ ions in MOCP **26**.

Given that MOCP **26** crystallizes in a chiral and polar space group *C*2 (point group $C_2$), experimental results indicate that MOCP **26** does indeed display ferroelectric behavior with a $P_r$ of 0.25 μC cm$^{-2}$

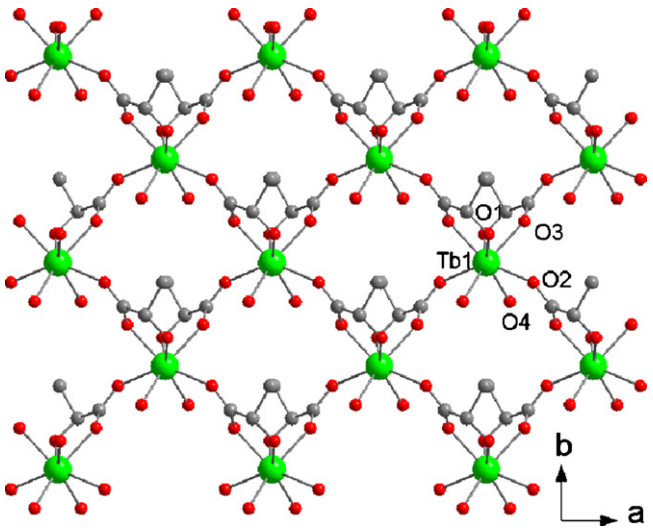


**Fig. 34.** Asymmetric unit view, 2D laminar and 3D homochiral framework in 2**6** [41].

and an $E_c$ of 0.2 kV cm$^{-1}$. On the other hand, the deuterated MOCP **26b** shows a $P_r$ of 0.90 μC cm$^{-2}$ and an $E_c$ of 0.33 kV cm$^{-1}$, reflecting a big DEF. MOCP **26** represents an example of metal-organic frameworks that exhibit ferromagnetic and ferroelectric properties together.

All of the homochiral or acentric MOCPs (**18**–**26**) definitely contain optically active organic ligands as building blocks. This suggests that the design and synthesis of potential ferroelectric MOCPs mainly depend upon the choice of homochiral organic ligands. For the construction of multiferroelectric MOCPs, transition metal ions should be used.

## 5. Conclusion and outlook

The search of ferroelectric MOCCs or MOCPs theoretically direct us to focus on the choice of homochiral or optically active organic ligands to prevent from no-purpose hard work like "Edisonian" approaches. This synthetic strategy is useful and efficient for screening polar MOCCs or MOCPs with desired functionalities. For the design of ferroelectric MOCCs, amino-acid-like ligands and alkaloids seem a good choice for the chirality. As to the non-H-bonded MOCCs, they should contain strongly distorted coordination geometries around the central ion with high-coordination number.

For development of new materials, molecular approach to modulate and combine properties is far more controllable and tunable than the atom-based solid state chemistry. MOCCs or MOCPs possess the advantages of the tunability of organic components and the diversity of inorganic components. With the aid of crystal engineering, metal-organic hybrid materials have been facing the blossom of molecule-based electronics. As to ferroelectric MOCCs or MOCPs, there have been several attempts for the development of theoretically and technologically important multiferroelectric MOCCs or MOCPs by combining spin carriers into the systems.

However, at present stage, the ferroelectric behaviors of the most MOCCs or MOCPs described here are still weak or "potential", which may be due to the rigid structures lacking mobility or inappropriate measurements. In fact, there are many reports giving out only shuttle-like electric hysteresis loops, which, however, generally do not serve as a sufficient proof for the existence of ferroelectricity [42]. It should be noted that, in order to confirm a ferroelectric behavior, one needs to take dielectric, DSC and crystallographic measurements further besides *P*–*E* measurement.

Although efforts have been put into the constructions of ferroelectric MOCCs or MOCPs, the realization of these kind of functional materials seems to be not easy and several aspects should be explored deeply. One is the investigation of the origin of ferroelectricity. As mentioned before, there are several mechanisms for conventional materials achieving ferroelectricity. But for MOCCs or MOCPs, due to their complexities in structures and components, it is hard to discriminate different ferroelectric origins. Possible mechanisms at present may include the structural distortion around the metal center and motion or distortion of small counterions. Furthermore, the identification of dipole inversion unit in the crystal lattice needs the synthesis of typical model compounds and detailed structural measurements.

Another tough task is the elucidation and utilization of phase transitions in MOCCs or MOCPs. It has been long found that phase transitions occur in most conventional ferroelectrics. Taking Rochelle salt for example, it experiences two-phase transition steps at 255 and 297 K, corresponding to paraelectric–ferroelectric and ferroelectric–paraelectric phase transitions, respectively. Generally speaking, the paraelectric phase is more symmetrical than the ferroelectric phase in the phase transition, which means ferroelectric–paraelectric transition is a symmetry-breaking process. It is possible to convert a central symmetric crystal to a polar ferroelectric crystal through paraelectric–ferroelectric phase transition by varying external stimuli such as temperature, pressure, etc. However, the prediction of the phase transition in MOCCs or MOCPs is much more difficult than it seems because of their complexity and the lack of knowledge on phase transition.

*Landau* theory of phase transition is a symmetry-based analysis of equilibrium behavior near a phase transition [43]. As a phenomenological approach, it can serve as a conceptual bridge between microscopic models and observed macroscopic phenomena. For the case of the paraelectric–ferroelectric transition, an order parameter, the polarization *P*, is used to characterize the transition. The free energy *F* in the vicinity of the transition is expanded as a *Taylor* expansion in terms of the order parameter *P* where only symmetry-compatible terms are retained. The state of the system is then found by minimizing this free energy $F(P)$ with respect to *P* to obtain $P_0$, and specific thermodynamic functions are subsequently computed by differentiating *F* accordingly. Successful applications of the theory can be found in some particular inorganic materials, which would shed light on the theoretical study of MOCCs or MOCPs.

In order to rationally design and synthesize ferroelectric MOCCs or MOCPs, one can utilize hydrogen transfer and motions of polar components and chiral centers to introduce electric polarizations. Taking hydrogen transfer for example, hydrogen bond is widely found in MOCCs or MOCPs and can be considered as a donor–acceptor system. It displays directional, but much weaker than covalent bonds binding atoms into molecules. Thus, the aggregates created through hydrogen bonds may easily undergo transformations by breaking and formation of alternative hydrogen bonds through proton transfer or proton order–disorder. Such transformations may change the properties of the corresponding crystals.

Multifunctional molecule-based materials have been attracting much attention in the material community, which stimulate the developments of new materials as well as new phenomena. The construction of multifunctional ferroelectric MOCCs or MOCPs is a challenging but promising task. Appealing multifunctional ferroelectric materials, which display coexistence or synergism with other physical (or chemical) properties, include magnetic, porous, chiral, photoresponsive, and optical materials. For example, the coexistence of both ferromagnetism and ferroelectricity sheds light on the new multifunctional material "multiferroics", which exhibits the prospect of controlling charges by applied magnetic fields and spins by applied voltages, and paves the way for construction of new forms of multifunctional devices [23].

## Acknowledgments

We thank 973 Project (Grant 2009CB623200) and National Natural Science Foundation of China as well as Jiangsu Province NSF (BK2008029). The former PhD and MS degree students are gratefully acknowledged for their distinct contributions.

## References

[1] J. Valasek, Phys. Rev. 17 (1921) 475.
[2] X. Solans, C. Gonzalez-Silgo, C. Ruiz-Pérez, J. Solid State Chem. 131 (1997) 350.
[3] (a) G. Busch, P. Scherrer, Naturwissenschaften 23 (1935) 737;
(b) G. Busch, Helv. Phys. Acta 10 (1937) 261;
(c) G. Busch, Ferroelectrics 71 (1987) 43.
[4] (a) B.M. Wul, I.M. Goldman, Dokl. Akad. Nauk SSSR 46 (1945) 154;
(b) B.M. Wul, I.M. Goldman, Compt. Rend. Acad. Sci. URSS 49 (1945) 139.
[5] A. von Hippel, R.G. Breckenridge, F.G. Chesley, L. Tisza, Ind. Eng. Chem. 38 (1946) 1097.
[6] (a) G. Shirane, K. Suzuki, A. Takeda, J. Phys. Soc. Jpn. 7 (1952) 12;
(b) G. Shirane, K. Suzuki, J. Phys. Soc. Jpn. 7 (1952) 333.
[7] G.H. Haertling, J. Am. Ceram. Soc. 82 (1999) 797.

[8] (a) K.M. Ok, E.O. Chi, P.S. Halasyamani, Chem. Soc. Rev. 35 (2006) 710;
(b) C.C. Homes, T. Vogt, S.M. Shapiro, S. Wakimoto, A.P. Ramirez, Science 293 (2001) 673.
[9] H. Zhang, X.M. Wang, K.C. Zhang, B.K. Teo, Coord. Chem. Rev. 183 (1999) 157.
[10] (a) B.T. Matthias, C.E. Millar, J.P. Remeika, Phys. Rev. 104 (1956) 849;
(b) M.E. Lines, A.M. Glass, Principle and Applications of Ferroelectrics and Related Materials, Clarendon Press, Oxford, 1977.
[11] H.-Y. Ye, D.-W. Fu, Y. Zhang, W. Zhang, R.-G. Xiong, S.D. Huang, J. Am. Chem. Soc. 131 (2009) 42.
[12] Y.-H. Li, Z.-R. Qu, H. Zhao, Q. Ye, L.-X. Xing, X.-S. Wang, R.-G. Xiong, X.-Z. You, Inorg. Chem. 43 (2004) 3768.
[13] (a) D.-W. Fu, Y.-M. Song, G.-X. Wang, Q. Ye, R.-G. Xiong, T. Akutagawa, T. Nakamura, P.W.-H. Chan, D.S.-P. Huang, J. Am. Chem. Soc. 129 (2007) 5346;
(b) H. Zhao, Z.-R. Qu, H.-Y. Ye, R.-G. Xiong, Chem. Soc. Rev. 37 (2008) 84.
[14] (a) S. Horiuchi, R. Kumai, Y. Tokura, J. Am. Chem. Soc. 127 (2005) 5010;
(b) I. Takasu, A. Izuoka, T. Sugawara, T. Mochida, J. Phys. Chem. B 108 (2005) 5527.
[15] (a) A.C. Pastor, R.C. Pastor, Ferroelectrics 71 (1987) 61;
(b) S. Koval, J. Kohanoff, J. Lasave, G. Colizzi, R.L. Migoni, Phys. Rev. B 71 (2005) 184102.
[16] Q. Ye, Y.-M. Song, D.-W. Fu, G.-X. Wang, R.-G. Xiong, P.W.-H. Chan, D.S.-P. Huang, Cryst. Growth Des. 7 (2007) 1568.
[17] X.-L. Li, K. Chen, Y. Liu, Z.-X. Wang, T.-W. Wang, J.-L. Zuo, Y.-Z. Li, Y. Wang, J.-S. Zhu, J.-M. Liu, Y. Song, X.-Z. You, Angew. Chem. Int. Ed. 46 (2007) 6820.
[18] C.-F. Wang, Z.-G. Gu, X.-M. Lu, J.-L. Zuo, X.-Z. You, Inorg. Chem. 47 (2008) 7957.
[19] (a) H. Zhao, Y.-H. Li, X.-S. Wang, Z.-R. Qu, L.-Z. Wang, R.-G. Xiong, B.F. Abrahams, Z.-L. Xue, Chem. Eur. J. 10 (2004) 2386;
(b) Q. Ye, Y.-Z. Tang, X.-S. Wang, R.-G. Xiong, Dalton Trans. (2005) 1570.
[20] Z.-R. Qu, H. Zhao, Y.-P. Wang, X.-S. Wang, Q. Ye, Y.-H. Li, R.-G. Xiong, B.F. Abrahams, Z.-G. Liu, Z.-L. Xue, X.-Z. You, Chem. Eur. J. 10 (2004) 54.
[21] Q. Ye, T. Hang, D.-W. Fu, G.-H. Xu, R.-G. Xiong, Cryst. Growth Des. 8 (2008) 3501.
[22] (a) P. Jain, N.S. Dalal, B.H. Toby, H.W. Kroto, A.K. Cheetham, J. Am. Chem. Soc. 130 (2008) 10450;
(b) H.F. Clausen, R.D. Poulsen, A.D. Bond, M.-A.S. Chevallier, B.B. Iversen, J. Solid State Chem. 178 (2005) 3342.
[23] W. Eerenstein, N.D. Mathur, J.F. Scott, Nature 442 (2006) 759.
[24] S. Ohkoshi, H. Tokoro, T. Matsuda, H. Takahashi, H. Irie, K. Hashimoto, Angew. Chem. Int. Ed. 46 (2007) 3238.
[25] K. Nakagawa, H. Tokoro, S. Ohkoshi, Inorg. Chem. 47 (2008) 10810.
[26] H.B. Cui, Z.M. Wang, K. Takahashi, Y. Okano, H. Kobayashi, A. Kobayashi, J. Am. Chem. Soc. 128 (2006) 15074.
[27] T. Okubo, R. Kawajiri, T. Mitani, T. Shimoda, J. Am. Chem. Soc. 127 (2005) 17598.
[28] Y.-M. Xie, J.-H. Liu, X.-Y. Wu, Z.-G. Zhao, Q.-S. Zhang, F. Wang, S.-C. Chen, C.-Z. Lu, Cryst. Growth Des. 8 (2008) 3914.
[29] L. Song, S.-W. Du, J.-D. Lin, H. Zhou, T. Li, Cryst. Growth Des. 7 (2007) 2268.
[30] W.-W. Zhou, J.-T. Chen, G. Xu, M.-S. Wang, J.-P. Zou, X.-F. Long, G.-J. Wang, G.-C. Guo, J.-S. Huang, Chem. Commun. (2008) 2762.
[31] H. Zhao, Z.-R. Qu, Q. Ye, B.F. Abrahams, Y.-P. Wang, Z.-G. Liu, Z.-L. Xue, R.-G. Xiong, X.-Z. You, Chem. Mater. 15 (2003) 4166.
[32] (a) Z.-R. Qu, Z.-F. Chen, J. Zhang, R.-G. Xiong, B.F. Abrahams, Z. Xue, Oganometallics 22 (2003) 2814;
(b) Q. Ye, S.-X. Wang, H. Zhao, R.-G. Xiong, Chem. Soc. Rev. 34 (2005) 208.
[33] W. Zhang, R.-G. Xiong, S.D. Huang, J. Am. Chem. Soc. 130 (2008) 10468.
[34] Y.-Z. Tang, X.-F. Huang, Y.-M. Song, P.W.-H. Chan, R.-G. Xiong, Inorg. Chem. 45 (2006) 4868.
[35] H. Zhao, Q. Ye, Z.-R. Qu, D.-W. Fu, R.-G. Xiong, S.D. Huang, W.P.H. Chan, Chem. Eur. J. 14 (2008) 1164.
[36] Y.-R. Xie, H. Zhao, X.-S. Wang, Z.-R. Qu, R.-G. Xiong, X. Xue, Z. Xue, X.-Z. You, Eur. J. Inorg. Chem. (2003) 3712.
[37] Z.-G. Gu, X.-H. Zhou, Y.-B. Jin, R.-G. Xiong, J.-L. Zuo, X.-Z. You, Inorg. Chem. 46 (2007) 5462.
[38] Q. Ye, Y.-M. Song, G.-X. Wang, K. Chen, D.-W. Fu, P.W.-H. Chan, J.-S. Zhu, D.S.-P. Huang, R.-G. Xiong, J. Am. Chem. Soc. 128 (2006) 6554.
[39] D.-W. Fu, W. Zhang, R.-G. Xiong, Dalton Trans. (2008) 3946.
[40] Z.-R. Qu, Q. Ye, H. Zhao, D.-W. Fu, H.-Y. Ye, R.-G. Xiong, T. Akutagawa, T. Nakamura, Chem. Eur. J. 14 (2008) 3452.
[41] Q. Ye, D.-W. Fu, H. Tian, R.-G. Xiong, P.W.H. Chan, S.D. Huang, Inorg. Chem. 47 (2008) 772.
[42] J.F. Scott, J. Phys. Condens. Matter 20 (2008) 021001.
[43] P. Chandra, P.B. Littlewood, arXiv: cond-mat/0609347 (2006).

## Glossary

*Dielectric:* A dielectric is a nonconducting substance.

*Piezoelectric:* A material generates an electric potential in response to applied mechanical stress.

*Pyroelectric:* A material generates an electric potential in response to a temperature change.

*Ferroelectric:* A material shows a spontaneous electric polarization that can be reversed by an external electric field.

*Current leakage:* It is a current flowing through the capacitor due to the dielectric material not being a perfect insulator and having some non-zero conductivity.

*Paraelectric phase:* It is a crystal phase in which electric dipoles are unordered and have the potential to align in an external electric field and strengthen it.

*Multiferroic:* A material exhibits more than one primary ferroic order parameter simultaneously, including ferromagnetism, ferroelectricity and ferroelasticity. However, many researchers in the field consider materials as multiferroics only if they exhibit coupling between the order parameters.